JBC RESEARCH ARTICLE

Alkaline pH has an unexpected effect on transcriptional pausing during synthesis of the *Escherichia coli* pH-responsive riboswitch

Received for publication, February 11, 2022, and in revised form, July 13, 2022 Published, Papers in Press, August 4, 2022,
https://doi.org/10.1016/j.jbc.2022.102302

Christine Stephen and Tatiana V. Mishanina*

From the Department of Chemistry and Biochemistry, University of California San Diego, La Jolla, California, USA

Edited by Craig Cameron

Riboswitches are 5′-untranslated regions of mRNA that change their conformation in response to ligand binding, allowing post-transcriptional gene regulation. This ligand-based model of riboswitch function has been expanded with the discovery of a "pH-responsive element" (PRE) riboswitch in *Escherichia coli*. At neutral pH, the PRE folds into a translationally inactive structure with an occluded ribosome-binding sequence, whereas at alkaline pH, the PRE adopts a translationally active structure. This unique riboswitch does not rely on ligand binding in a traditional sense to modulate its alternative folding outcomes. Rather, pH controls riboswitch folding by two possible modes that are yet to be distinguished; pH either regulates the transcription rate of RNA polymerase (RNAP) or acts on the RNA itself. Previous work suggested that RNAP pausing is prolonged by alkaline pH at two sites, stimulating PRE folding into the active structure. To date, there has been no rigorous exploration into how pH influences RNAP pausing kinetics during PRE synthesis. To provide that understanding and distinguish between pH acting on RNAP *versus* RNA, we investigated RNAP pausing kinetics at key sites for PRE folding under different pH conditions. We find that pH influences RNAP pausing but not in the manner proposed previously. Rather, alkaline pH either decreases or has no effect on RNAP pause longevity, suggesting that the modulation of RNAP pausing is not the sole mechanism by which pH affects PRE folding. These findings invite the possibility that the RNA itself actively participates in the sensing of pH.

Organisms implement a diverse array of strategies to tune their gene expression programs in response to changing environmental conditions. One such tuning strategy employed by bacteria is the use of riboswitches—structured 5′-untranslated regions of an mRNA that dictate whether the downstream gene is transcribed and/or translated into protein. Riboswitches typically regulate gene expression by altering their structure upon binding to a nutrient ligand (*e.g.*, metal ions, amino acids, vitamins) (1). A pH-responsive riboswitch discovered in *Escherichia coli*, however, does not require a ligand-binding event in a traditional sense to rearrange its structure and instead rearranges its structure in response to the environmental H^+ concentration. This riboswitch is a "pH-responsive element" (PRE): at neutral pH, the PRE folds into a translationally inactive structure with an occluded ribosome binding sequence (RBS), whereas at alkaline pH, the PRE adopts a translationally active structure with an exposed RBS (2). This conformational isomerization regulates the expression of the downstream gene, which encodes a putative metal transporter that is highly upregulated under *ex*treme *al*kaline conditions, thus called "*alx*" (Figs. 1 and S1) (3).

The *alx* gene was first identified in a genetic screen seeking *E. coli* genes that are upregulated in response to alkaline conditions (3). Later, a screen for small RNAs with potential regulatory function in *E. coli* uncovered a small RNA termed SraF that is immediately upstream of the *alx* gene (also known as *ygjT* gene) (4). Upon further investigation, SraF was definitively characterized as a pH-responsive riboswitch controlling translation of the *alx* mRNA through a combination of *lacZ* reporter fusion assays and RNA chemical probing experiments performed both *in vitro* and *in vivo* (2). The pH-responsive riboswitch is generally conserved amongst bacteria in the *Enterobacteriales* order (2), a large and diverse group of Gram-negative bacteria that have been found in soil, water, and in association with living organisms (5)—all of which are environments where bacteria can experience an external alkaline pH (6). It appears that the *alx* gene and its control by the PRE has arisen to help counter the stress imposed on bacteria upon a shift into an external alkaline environment that can be encountered in their ecological niches. While non-extremophilic bacteria deploy a wide range of strategies to maintain the cytoplasmic pH in a neutral range (generally 7.4–7.8), previous experiments measuring the cytoplasmic pH of log-phase *E. coli* after a rapid shift to an alkaline medium demonstrated that the cytosol alkalinizes before recovering the desired neutral pH (7). Thus, the PRE (and RNA polymerase transcribing it) can experience an alkaline environment *in vivo* to prompt its structural rearrangement and increase translation of the Alx protein. The Alx protein is a member of the TerC family of membrane transporter proteins and has been implicated in Mn^{2+} transport (8); however, the connection between Mn^{2+} transport activity and alkaline pH awaits elucidation. In addition, the molecular mechanisms

* For correspondence: Tatiana V. Mishanina, tmishanina@ucsd.edu.

underpinning the pH-dependent riboregulation of the *alx* gene remain unknown.

Previous studies suggest that PRE folding is kinetically controlled. Specifically, the model for PRE folding proposed that RNA polymerase (RNAP) pausing—a temporary inhibition of nucleotide (nt) addition during transcript elongation—is enhanced by alkaline pH at two specific sites during PRE synthesis, which promotes folding of the PRE into the active structure (Fig. 1*B*) (2, 9). Two key pieces of evidence supported this model. First, unfolding of RNA synthesized at neutral pH, followed by refolding at alkaline pH did not produce the translationally active conformer, which indicates that pH exerts control over PRE folding cotranscriptionally (2). Second, RNA made by T7 RNAP (which in general pauses minimally during transcription) (10) assumed the same inactive structure at either neutral pH or alkaline pH (2). While these observations support the importance of strategically placed transcriptional pauses to the RNA-folding outcome, they do not distinguish between the two possible mechanisms of pH action: (i) pH altering paused RNAP structure to prolong its residence time at the key pause sites *versus* (ii) pH acting on the RNA to favor its cotranscriptional folding into the active conformer.

Pausing by RNAP plays crucial regulatory roles in both prokaryotes and eukaryotes by creating windows of time for regulatory events. In addition to allowing transcriptional regulators to (un)bind to RNAP, pausing in bacteria allows synchronization of transcription and translation, promotes the proper folding of nascent RNA transcripts, and is an initial step in transcription termination (11). Previous studies of *E. coli* RNAP have elucidated key structural changes in the enzyme when it reaches DNA sequences that induce pausing (12). These structural changes rearrange the active site of RNAP into a conformation that cannot catalyze nt addition. Despite these advances, it remains unclear how RNAP pausing might be prolonged as it transcribes the *same* sequence of DNA at alkaline pH compared with neutral pH in the context of the PRE. To address this gap in knowledge, we performed the first rigorous exploration into how pH influences RNAP pausing during PRE synthesis. An improved understanding of the kinetic control mechanism underlying pH-dependent riboswitching would both enrich our basic knowledge of kinetically controlled riboswitches and facilitate its use as an engineerable switch for synthetic gene circuits, which have various biotechnological applications, ranging from biosynthesis of antibacterial drugs to biofuel production (13).

Our experiments revealed that the first and most critical pause site for RNA folding, termed "pause 1" in the originally published work, is actually a composite of three sequential pauses.

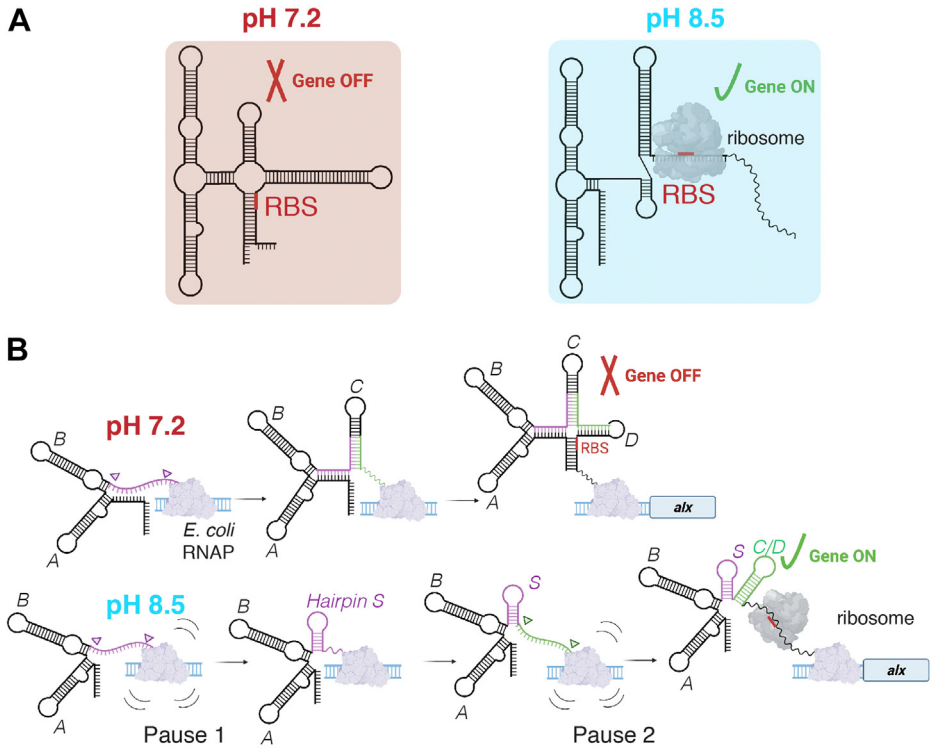

Figure 1. Alternative folding outcomes of the pH-responsive riboswitch. *A*, overview of the pH-responsive riboswitch folding outcomes under different pH conditions. When the PRE is synthesized under conditions of alkaline pH, a translationally active structure is formed with the ribosome binding sequence (RBS) available for ribosome binding and subsequent translation, turning on the downstream gene (*alx*). When the PRE is synthesized under conditions of neutral pH, a translationally inactive structure is formed with the RBS occluded, turning off the *alx* gene. The PRE structure models presented here are based on previously published structure predictions, which were generated *via* chemical probing with dimethyl sulfate (DMS) followed by primer extension (2). *B*, proposed folding pathways for the pH-responsive riboswitch under both alkaline and neutral pH. The folding pathways shown illustrate the PRE folding model proposed by Nechooshtan *et al.* (2). Under alkaline conditions, it was proposed that RNAP pause longevity is enhanced at two key sites to promote folding of specific structural elements in the active conformer (hairpin S and hairpin C/D, shown in *purple* and *green*, respectively). The *colored arrows* denote the RNA portions that alternatively base pair to form hairpin S and hairpin C/D in the active conformer. PRE, pH-responsive element; RNAP, RNA polymerase.

Furthermore, measurements of RNAP pausing kinetics at these pauses showed that pH impacts pause longevity but not in the previously proposed manner. Rather, alkaline pH either accelerates or has no effect on RNAP pause escape. In addition, we explored RNAP pausing kinetics at "pause 2," the second critical decision point for the RNA folding. At this site, we find that alkaline pH accelerates the pause escape rate. Taken together, our findings suggest that modulation of RNAP pausing alone is insufficient to explain the alternative PRE folding outcomes under different pH. We posit that the RNA is involved in sensing and rearranging its structure in response to alkaline conditions.

Results

Alkaline pH accelerates E. coli *RNAP transcription through the pH-responsive riboswitch*

To monitor the transcription progress of *E. coli* RNAP under neutral *versus* alkaline pH on the full PRE sequence, we performed synchronized single-round *in vitro* transcription assays initiated at the native promoter that controls PRE synthesis *in vivo* (see Fig. S2, *A* and *B* for detailed DNA template sequence and experimental scheme). The transcription time courses demonstrated that *E. coli* RNAP transcribes through the PRE sequence faster under alkaline pH conditions relative to neutral pH (Fig. 2, *B* and *C*). This observation is consistent with the chemical mechanism of nt addition, where in the first step a base in the RNAP active site deprotonates the 3′ hydroxyl of the terminal nt on the RNA transcript (Fig. 2*A*). Therefore, as pH alkalinizes, the fraction of the catalytic base in the deprotonated form increases, explaining the observed increase in the transcription rate. This observation is also consistent with previous experimental analysis of *E. coli* RNAP transcription kinetics under different pH conditions (14). Although alkaline pH clearly enhances the average transcription rate (Fig. 2*C*), these measurements do not directly address the question of pause longevity, which may be obscured by other events in the transcription elongation assay. The prevailing PRE folding model proposes that RNAP pause escape is *slowed* at alkaline pH *versus* neutral pH to support folding of specific structural motifs in the active PRE conformer.

We observed pausing on the PRE sequence at similar positions to those reported in the original work (Fig. 2*B*) (2). To begin, we analyzed the pause site termed "pause 1," which was identified as the first critical pause location for PRE folding. Specifically, it was proposed that prolonged pausing at this site at alkaline pH provides a time window for folding of "hairpin S," a key structural element in the PRE active conformer (Fig. 1*B*; see Fig. S1 for PRE secondary structure models at different pH and Table S1 for PRE sequence) (2). First, we find that the RNA band identified as "pause 1" in previous work is actually a composite of three sequential pause RNA species (Fig. 3*B*). We analyze the reasons for the discrepancy in the following section, and for consistency with prior work, we will continue to refer to this composite of three pauses collectively as "pause 1." We estimated the average dwell time of RNAP at pause 1 by treating the diffuse band as a single RNA species, following established methodologies to determine pause kinetic parameters (15, 16). Since RNAP arrives at pause 1 more rapidly at pH 8.5 *versus* 7.2, we fit kinetic parameters to data points where continued arrival of RNAP at the pause was negligible (10–20 s for pH 7.2 and 8–12 s for pH 8.5). This analysis yielded average pause dwell times of 13 s at pH 7.2 and 9 s at pH 8.5 (Fig. S2*C*), suggesting that, in contrast to the prevailing model, RNAP resides at pause 1 for longer under neutral conditions. However, these promoter-initiated data did not permit individual kinetic treatment of each sequential pause comprising pause 1; therefore, it was unclear whether each pause lifetime was longer under neutral conditions or if a single pause RNA species in the diffuse band was biasing the results. To truly address whether alkalinity prolongs RNAP pausing at the first, and most important site for PRE folding into the active conformer, we employed scaffold-based transcription assays, described in the subsequent sections.

The prevailing PRE folding model proposes that an additional pause in the folding pathway, "pause 2," is prolonged by alkaline pH to support folding of hairpin C/D in the active conformer (Figs. 1*B* and S1) (2). We observed multiple pause RNA species in the expected region for pause 2 prior to the termination site D (Fig. 2*B*, see the next paragraph for description of termination sites on PRE). Similar to our analysis of pause 1, we fit kinetic parameters to data points where continued arrival of RNAP at the pause was negligible (14–20 s for pH 7.2 and 8–12 s for pH 8.5). This analysis yielded average pause dwell times of 11 s at pH 7.2 and 7 s at pH 8.5 (Fig. S2*C*), suggesting that RNAP also resides at pause 2 for longer under neutral conditions. These data, however, present the same limitations addressed in our analysis of pause 1, prompting us to explore the kinetics of pause 2 further with scaffold-based transcription assays that are also described in the subsequent sections.

Besides pause 1 and 2 sites, the other prominent RNA species observed in this experiment (∼108 nt and ∼190 nt) correspond to intrinsic termination sites (Fig. 2*B*). Intrinsic termination occurs when an RNA hairpin forms in the RNAP exit channel while RNAP is positioned on an unstable RNA–DNA hybrid, prompting dissociation of the elongation complex (EC) (17). Hairpins B and D in the PRE are characteristic intrinsic terminator hairpins with hairpin structures followed by a U-tract (Fig. S1); for consistency with prior work, we will refer to these termination sites as termination site B and termination site D, named for their respective hairpin structures. A slightly larger fraction of ECs terminated at site B at neutral pH (Fig. S2*C*), with ∼46% of ECs terminating here at pH 7.2 and ∼43% of ECs at pH 8.5. A slightly larger fraction of ECs terminated at site D at neutral pH (Fig. S2*C*), with ∼13% of ECs terminating here at pH 7.2 and ∼10% of ECs at pH 8.5. The RNA species corresponding to termination sites B and D persist in the "chase" lane (Fig. 2*B*), which represents a 5-min reaction at saturating NTPs (500 μM). Thus, these locations are definitively termination sites and not long-lived pauses.

Modulation of RNAP pausing by transcription factors during synthesis of the pH-responsive riboswitch

To gain further insights into the nature of the pauses, we performed transcription elongation assays in the presence of

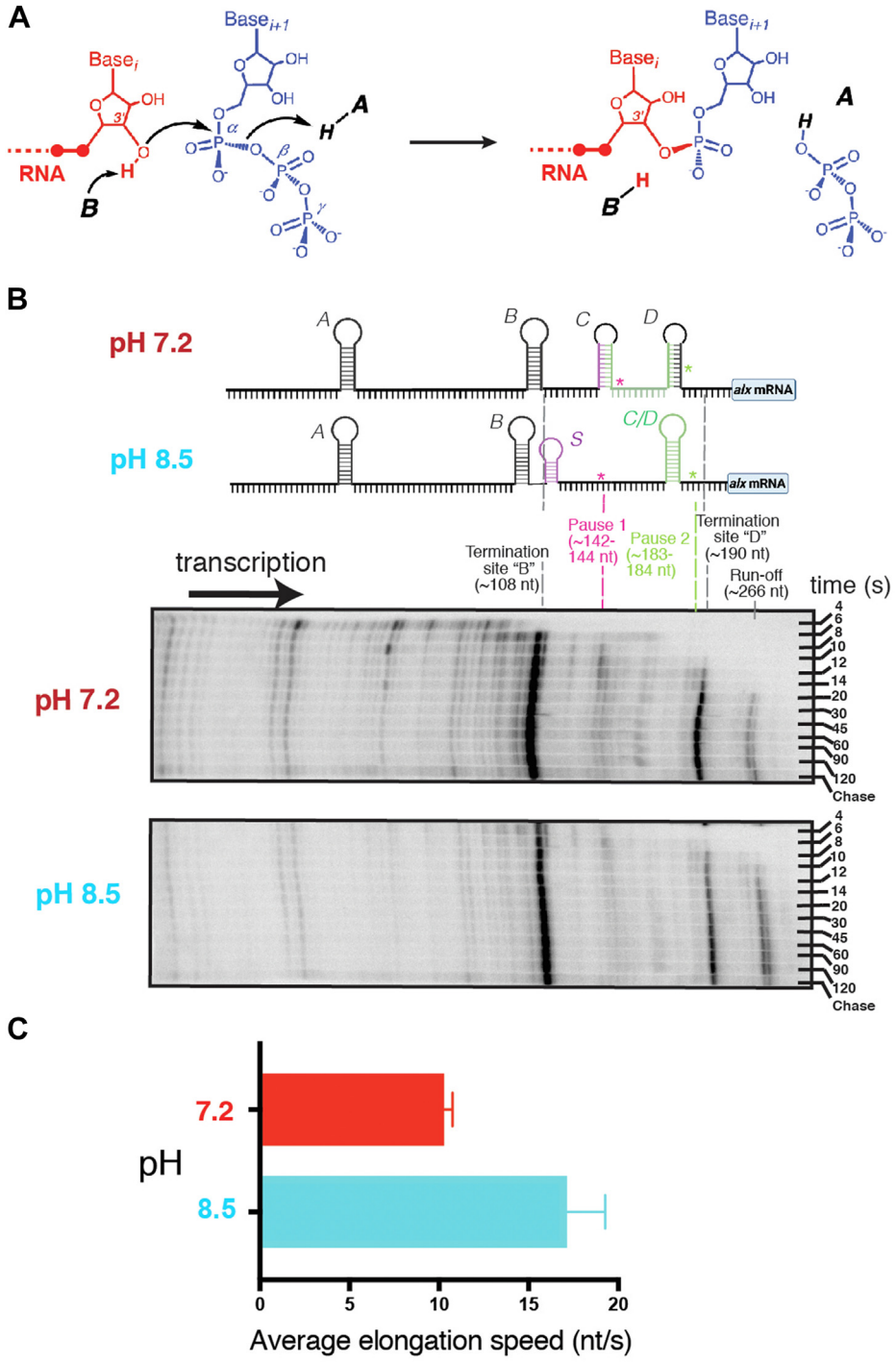

Figure 2. RNAP transcription through the PRE at neutral *versus* alkaline pH. *A*, chemical mechanism of nucleotide addition by RNAP. The flow of electrons in the reaction is marked with *arrows*. Proton abstraction and donation are performed by the putative base (B) and acid (A), respectively. *B*, synchronized single-round *in vitro* transcription from the *alx* promoter upstream of the PRE. Transcription progress was monitored at pH 7.2 and 8.5. RNA transcripts were radiolabeled *via* incorporation of [α-^{32}P]ATP and visualized on a 10% denaturing polyacrylamide gel. Prominent RNA species are labeled with approximate transcript lengths. *C*, average transcription rate of *Escherichia coli* RNAP on the PRE at pH 7.2 *versus* pH 8.5. Error shown is SD of a triplicate measurement. PRE, pH-responsive element; RNAP, RNA polymerase.

E. coli transcription factors known to modulate pausing. We first tested for backtracked pauses by including the transcription factor GreA during *in vitro* promoter-initiated transcription assays at different pH. A backtracked pause is a long-lived pause that occurs when RNAP reverse translocates on the RNA–DNA hybrid and extrudes the 3′-end of the RNA through its secondary channel, thereby precluding an incoming NTP from entering the active site (11). GreA relieves RNAP from a backtrack by stimulating cleavage of the extruded 3′-RNA piece, permitting RNAP to continue transcription elongation

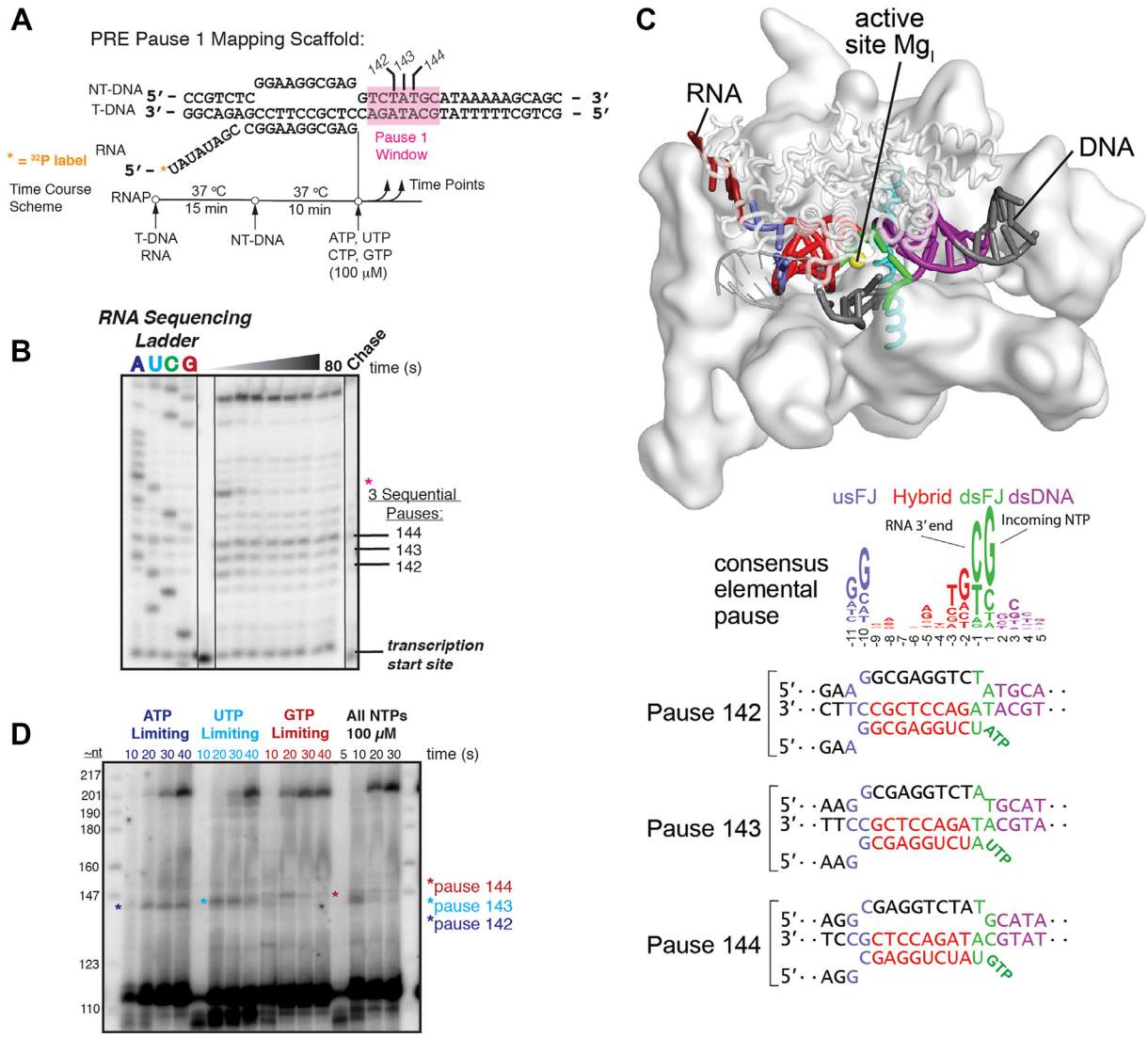

Figure 3. Locating the first critical pauses for PRE folding. *A*, experimental overview for mapping the first critical pause ("pause 1") in the PRE folding pathway. *B*, pause mapping. RNA sequencing ladder generated using corresponding 3′-deoxyNTP. Time-course samples were run alongside sequencing ladder for precise identification of the pause locations. Pause band numbering denotes nucleotide position on the PRE. All pause bands disappear after 5 min with saturating NTP ("chase" lane), indicating these do not result from arrested transcription complexes and indeed represent transient PECs. The *asterisk* (*) denotes a pause RNA band downstream of the sequential pauses most likely introduced by shortening of the downstream DNA. The splice borders denote samples that were not adjacent to one another in the original gel image. *C*, sequence comparison of PRE sequential pauses to the consensus elemental pause. *Top panel*, the ePEC structure (Protein Data Bank ID: 6BJS; representation adapted from reference 28) (12, 28) is shown above the consensus elemental pause sequence logo identified *via* NET-seq (27), represented as the nucleotide sequence of the nontemplate DNA. The ePEC structure and sequence logo have the following color scheme: upstream fork junction (usFJ, *blue*), hybrid (*red*), downstream fork junction (dsFJ, *green*), and downstream DNA (dsDNA, *purple*). Numbering corresponds to position relative to the RNA 3′ end at the RNAP active site. *Bottom panel*, PRE pause sequences with color scheme to match that used for the pause consensus to facilitate sequence comparison. *D*, synchronized single-round *in vitro* transcription from the *alx* promoter to visualize the sequential pauses. Transcription elongation reactions were performed with one NTP at a limiting concentration (20 μM) to slow pause escape, permitting visualization of each pause in the sequential series. Each pause RNA band is denoted with an *asterisk* (*). Radiolabeled RNA samples were separated on a 10% denaturing polyacrylamide gel. ePEC, elemental paused elongation complex; PEC, paused elongation complex; PRE, pH-responsive element.

(18, 19). GreA exerts a clear effect at the pause 1 site under both neutral and alkaline conditions by consolidating the multiple RNA bands observed at pause 1 into a single band, which persists at later time points relative to the no-factor condition (Fig. S2*D*). This suggests that a backtracking event occurs at pause 1, which we confirmed with scaffold-based transcription assays outlined in later sections.

We next included the transcription factor NusA into *in vitro* transcription elongation assays to expose potential hairpin-stabilized pauses. Hairpin-stabilized pauses occur when an RNA hairpin in the RNAP exit channel extends pause longevity (11) and are enhanced in the presence of NusA through stabilizing contacts between NusA and paused RNAP (20). Previous work supported the existence of hairpin-stabilized pauses at both pause 1 and pause 2 (2); however, reproducibility and gel quantification of these results were not reported. We first performed promoter-initiated transcription elongation assays in the presence of 500 nM NusA, matching the concentration used in previously reported experiments (2). In our experiments, we observed multiple putative hairpin-

stabilized pauses prior to termination site B that are enhanced by NusA as well as increased termination at site B (Fig. S2*E*). We also noticed a significant decrease in transcription elongation past the termination site B at 500 nM NusA such that pauses 1 and 2 were not detected (Fig. S2*E*), in stark contrast to previous work (2). This is likely caused by NusA stabilization of the intrinsic terminator hairpin at termination site B, increasing the fraction of ECs that dissociate here.

In an attempt to observe transcription and the pauses past termination site B, we performed transcription elongation assays with NusA present at lower concentrations (50, 100, and 250 nM). The effect of NusA at 100 and 250 nM mimics that seen with the 500 nM condition, with multiple pauses enhanced by NusA and increased termination at termination site B, but not many transcripts produced beyond that point (Fig. S2*E*). At 50 nM NusA, we observe sufficient elongation past termination site B to visualize pauses 1 and 2; however, we cannot visualize enhancement of the pauses prior to termination site B (Fig. S2*E*), suggesting that the 50 nM concentration of NusA is insufficient to observe pause enhancement in this experiment.

Further gel analysis of transcription elongation time courses with NusA suggests that three hairpin-stabilized pauses reside at positions C36, C58, and C73/A74 on the PRE (Figs. S2*F* and S1). At positions C73/A74, hairpin A is appropriately spaced from the RNAP active site such that it could reside in the RNA exit channel and prompt a hairpin-stabilized pause (Fig. S1; see Fig. S7*A* for an example of appropriate spacing in the context of a well-studied *his* pause). At positions C36 and C58, there are no hairpin structures present in the fully folded RNA to rationalize the observed enhancement of these pauses in the presence of NusA. Nevertheless, it is possible the PRE traverses through labile folding intermediates during its synthesis similarly to other noncoding RNAs (21–23) and riboswitches in particular (24–26), thus the putative hairpins present in the RNAP exit channel at positions C36 and C58 cannot be visualized in the fully folded RNA structure. Prior work on the pH-responsive riboswitch reported that NusA promotes formation of the active PRE conformer under neutral conditions, mimicking the effect of alkaline pH (2). Since we cannot find evidence for hairpin-stabilized pauses in the critical region for pH-responsive riboswitching, it is unclear how NusA produced this effect.

Three sequential pauses constitute the first critical decision point for pH-responsive riboswitch folding

To assess RNAP pausing on the PRE under different pH conditions, we performed a different class of transcription assay that bypasses the need for initiating transcription from a promoter and zooms in on the locations of the pauses, thus simplifying kinetic analysis. We first positioned RNAP on a short synthetic nucleic acid scaffold corresponding to the reported location of pause 1 (2, 9), which was reportedly prolonged by alkaline pH to promote the folding of hairpin S in the PRE active conformer (Figs. 1*B* and S1). To test whether the pause escape rate at this site is slowed by alkaline pH, we measured the escape rate of *E. coli* RNAP from this proposed pause under neutral *versus* alkaline pH conditions. Under both pH conditions, rapid RNA extension was observed (Fig. S3*A*), which is behavior indicative of an active EC rather than a paused elongation complex (PEC). Therefore, this experiment demonstrated that the location of pause 1 was originally mapped incorrectly, likely because of limited resolution of the gel analysis of long RNAs produced from promoter-initiated transcription.

To elucidate the sequence motifs responsible for the pauses, we performed a scaffold-based transcription assay that positioned the ECs upstream of the sequence window where pause 1 lies (Fig. 3*A*). An RNA sequencing ladder was generated for precise assignment of the pause site. These experiments located pause 1 ∼4 nt downstream of the originally published site and uncovered that the paused RNA species termed "pause 1" in the originally published work is a composite of three sequential pauses (Fig. 3*B*). In the original RNA gel analysis, which employed a 6% denaturing PAGE, these paused RNAs migrated as a single diffuse band. We also observed this diffuse band on our 6% gels (Fig. S2*B*). To ensure that these sequential pauses are the biologically relevant ones, and not an artifact from using a minimalistic transcription scaffold, we clearly captured the sequential pauses in promoter-initiated transcription experiments (Fig. 3*D*). Specifically, each of the sequential pause RNA species was observed by limiting the incoming NTP at each of the respective pause sites and analyzing RNA products on a 10% (*versus* originally used 6%) denaturing PAGE, which allowed nt resolution in the region of the gel where the pause RNA species migrate. We also performed the scaffold-based pause mapping experiment with limiting NTP conditions and observed an increase in pause duration at each sequential pause site (Fig. S3*B*).

We compared the sequential pause sequences to the consensus elemental pause sequence (Fig. 3*C*), which was previously identified using high-throughput sequencing of nascent RNAs from bacteria (NET-seq) (27). The pauses at positions 142 and 143 on the PRE sequence lack the −1 CG base pair (bp) and +1 GC bp present in the consensus sequence. However, the pause at 142 shares the −10 GC bp with the consensus sequence, and the pause at 143 shares both the −10 and −11 GC bp with the consensus sequence. Finally, the pause at position 144 on the PRE sequence shares the +1 GC bp and −11 GC bp with the consensus sequence. Previous kinetic analyses of *E. coli* RNAP on the consensus elemental pause sequence have demonstrated that the pause signal is multipartite, with individual sequence elements having an additive effect on overall pause strength (28). Therefore, all elements of the consensus pause sequence are not necessary to observe a pause, as seen with the sequential pauses we identified on the PRE. Furthermore, to assess whether the newly mapped pauses at positions 142 to 144 on the PRE sequence occur *in vivo*, we analyzed the previously reported NET-seq data for the entire *E. coli* genome (27). From these data, three peaks are observed at the genomic locations corresponding to positions 142 to 144 on the PRE (Fig. S3*C*), supporting their existence *in vivo*.

E. coli *RNAP pause longevity is either decreased or unaffected by alkaline pH at the first major pause sites in the pH-responsive riboswitch folding pathway*

To test whether RNAP pausing is prolonged by alkaline pH at the sequential pauses, we reconstituted ECs at each of the sequential pause sites and measured the "elemental" pause lifetimes at neutral and alkaline pH. When RNAP first encounters a pause signal in the transcribed nucleic acids, it rearranges into an elemental paused elongation complex (ePEC), entering into a transient catalytically inactive state (Fig. 3*C*) (28). Depending on the sequence, the ePEC can either return to an active elongation conformation or isomerize into a longer-lived pause state such as a backtracked or a hairpin-stabilized pause described in the earlier section. In these experiments, we focused solely on elemental pause longevity (without upstream RNA structure) and its response to pH because the elemental pause is an obligate precursor for longer-lived pauses that may mediate PRE folding. This setup permitted direct evaluation of the alkaline pH effect on the paused RNAP and thus the proposed PRE folding model. An evaluation of the proposed folding model could not be performed based on promoter-initiated transcription experiments alone for the following reasons: (i) the elemental pause longevities could not be measured since the full-length nascent RNA is present and (ii) promoter-initiated experiments did not permit rigorous kinetic treatment of each individual pause in the sequential series because of poor resolution of pause bands on the gel and large number of other RNA species present. Kinetic and structural analyses of PECs reconstituted on synthetic nucleic acid scaffolds have enriched our fundamental understanding of transcriptional pausing (12, 28, 29), prompting our application of scaffold-based transcription assays to study the PRE pauses here.

In our experiments, ECs were assembled on synthetic nucleic acid scaffolds corresponding to each sequential pause that contain a fully complementary transcription bubble. The 5′ radiolabeled RNA primer used for each scaffold was 17-nt in length with an 11-nt region of complementarity (to form an RNA–template DNA [T-DNA] hybrid) and a 6-nt noncomplementary 5′-tail mimicking nascent RNA in the RNA exit channel of RNAP. Additional complementarity was not introduced in the upstream RNA segment to prevent ECs from assembling at an undesired location upstream of the pauses. Following PEC assembly, we measured the fraction of pause RNA over time at pH 7.2 and 8.5 when the radiolabeled PECs were extended with the NTP required for pause escape. To obtain kinetic parameters, a semilogarithmic plot was generated for the pause RNA fraction over time, and a single-exponential decay fitting was performed on the plot (Fig. S4*A*). At the first pause, pause decay was faster at alkaline pH, with an average RNAP dwell time at the pause of 54 s at pH 8.5 *versus* 174 s at pH 7.2 (Fig. 4*A* and Table S2). At the second pause in the sequential series, the average pause dwell time was 33 s at pH 7.2 *versus* 34 s at pH 8.5, demonstrating a similar RNAP residence time at this pause at both pH (Fig. 4*B*). At the third pause, pause decay was faster at alkaline pH, with an average pause dwell time of 16 s at pH 8.5 and 32 s at pH 7.2 (Fig. 4*C*). However, the calculated dwell times for the third pause do not accurately depict the pause escape rate since a large fraction of the ECs is inactivated, evidenced by the significant remaining fraction of PECs after incubation with a saturating concentration of the incoming NTP. We demonstrated that ECs remaining at the third pause are backtracked (see Supporting Discussion section), with a backtracking event prompted by the presence of a destabilizing AU-rich DNA–RNA hybrid—a sequence motif known to promote backtracking (11, 30). Besides the backtracking event at the third pause, in general we observed RNA products resulting from intrinsic cleavage of ECs positioned at each pause, which are characterized and analyzed in detail in the Supporting Discussion section.

Taken together, the sequential pause lifetimes observed in our scaffold experiments are significantly longer than those calculated from promoter-initiated transcription experiments, which can be attributed to multiple factors. The shortened downstream DNA in scaffold experiments compared with promoter-initiated experiments likely increased pause lifetimes, an observation consistent with prior analyses of *E. coli* RNAP pausing (31). This, for example, is consistent with reported kinetic analyses of the *his* pause—a well-characterized hairpin-stabilized pause in the leader region of the histidine biosynthetic operon—in a promoter *versus* scaffold-based transcription experiments (12, 15). The absence of the nascent riboswitch RNA in scaffold experiments also presumably affected the details of observed pausing kinetics. In particular, a significant fraction of RNAP cannot escape the backtrack at position 144 in our scaffold experiments (Fig. 4*C*); however, when the full-length nascent RNA is present in promoter-initiated experiments, the pause RNA species at 142 to 144 largely disappear after 30 s (Fig. 2*B*). This agrees with previous reports that highlight cotranscriptionally folded RNA imposing a kinetic barrier to RNAP backtracking (32, 33). Although there are clear differences in pause longevity between the scaffold and promoter-initiated experiments, the general effect of pH on pause kinetics was consistent: the average time RNAP spends at any of the individual sequential pauses, or at pause 1 collectively, is not increased by alkaline pH.

While the aforementioned scaffold experiments provided a useful initial characterization of the sequential pauses, many open questions remained regarding how pH influences RNAP pausing. For example, these scaffold experiments only permitted evaluation of pause lifetimes and not pause efficiencies—a parameter that describes the fraction of RNAP molecules captured by a particular pause sequence (34). In addition, these experiments lacked a complete characterization of the backtracking event at the third pause. Experiments positioning ECs directly at the sequential pauses outlined here *suggest* that PECs enter a backtracked register at the third pause; however, these data could not provide a comprehensive depiction of both the backtracked register and the pause escape kinetics when ECs encounter this pause during active transcription elongation. To address these limitations and provide a precise dissection of how pH modulates both pause

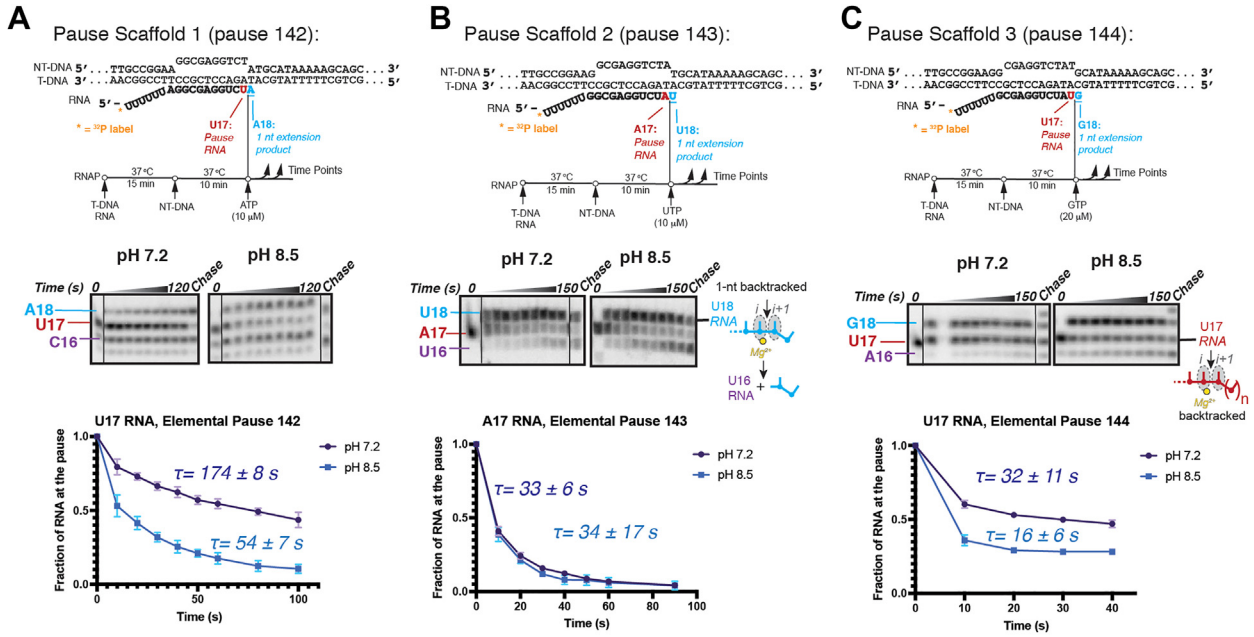

Figure 4. Measurements of elemental pause escape rate at the sequential pauses under neutral *versus* alkaline conditions. *A*, elemental pause escape measurements at pH 7.2 and pH 8.5 for the first pause in the sequential series downstream of hairpin S. *Top panel*, experimental overview of pause escape experiment. PECs were preformed by positioning RNAP on the nucleic acid scaffold shown. The rate of RNA extension was measured after addition of ATP. Time points were taken at regular intervals ranging from 0 s to 120 s. *Middle panel*, representative gel images from transcription time courses. "Chase" represents a sample taken after allowing elongation to proceed for 5 min with saturating ATP. *Bottom panel*, results from gel quantification of the pause RNA fraction over time at pH 7.2 *versus* 8.5. Error is SD of triplicate. Average dwell time at the pause at each pH is specified. The splice borders denote samples that were not adjacent to one another in the original gel image. *B*, elemental pause escape measurements at pH 7.2 and pH 8.5 for the second pause in the sequential series downstream of hairpin S. *Top panel*, the rate of RNA extension was measured after addition of UTP. Time points were taken at regular intervals ranging from 0 s to 150 s. *Middle panel*, representative gel images from transcription time courses. "Chase" represents sample taken after allowing elongation to proceed for 5 min with saturating UTP. *Cartoon* adjacent to gel image depicts a 1-nt backtracking and intrinsic cleavage event that occurs following incorporation of UMP by ECs positioned at the second pause. *Bottom panel*, results from gel quantification of the pause RNA fraction over time at pH 7.2 *versus* 8.5. Error is SD of triplicate. Average dwell time at the pause at each pH is specified. The splice borders denote samples that were not adjacent to one another in the original gel image. *C*, elemental pause escape measurements at pH 7.2 and pH 8.5 for the third pause in the sequential series downstream of hairpin S. *Top panel*, the rate of RNA extension was measured after addition of GTP. Time points were taken at regular intervals ranging from 0 s to 150 s. *Middle panel*, representative gel images from transcription time courses. "Chase" represents sample taken after allowing elongation to proceed for 5 min with saturating GTP. *Cartoon* adjacent to gel image depicts that ECs positioned at the third pause enter a backtracked register; the precise translocation register could not be ascertained in this experiment, hence the "n" notation next to the extruded RNA piece. *Bottom panel*, results from gel quantification of the pause RNA fraction over time at pH 7.2 *versus* 8.5. Error is SD of triplicate. Average dwell time at the pause at each pH is specified. The splice borders denote samples that were not adjacent to one another in the original gel image. EC, elongation complex; PEC, paused elongation complex; RNAP, RNA polymerase.

escape and pause efficiency at the sequential pauses, we performed additional scaffold-based transcription assays described in the next section.

Gre factor–stimulated RNA cleavage increases traffic through the sequential pauses

To further investigate both the backtracking at the third pause and the sequential pauses in general, we performed additional scaffold-based transcription assays where RNAP arrived at each pause during active transcription elongation *versus* positioned directly at the pause, as in the preceding section. These experiments permitted evaluation of both pause lifetimes and pause efficiencies at different pH in the presence and absence of Gre factors (Table S3). Briefly, we reconstituted ECs on a synthetic DNA–RNA scaffold corresponding to position 136 on the PRE (G10 ECs), and the G10 ECs were radiolabeled *via* incorporation of [α-^{32}P] ATP, extending the RNA to form A11 ECs (Fig. 5*A*). Transcription elongation was then initiated upon addition of all four NTPs to the A11 ECs, with the incoming NTP at the pause being analyzed present at a limiting concentration. Limiting the incoming NTP at each pause increased the pause duration and permitted manual quenching. Similar to the analysis performed in the previous section, a semilogarithmic plot was generated for the pause RNA fraction over time and a single-exponential decay fitting was performed on the plot.

Pause 144 analysis

We first performed transcription elongation assays at a limiting concentration of GTP (20 μM) to increase the duration of the third pause and evaluate how pH affects both the pause lifetime and pause efficiency in the presence and absence of Gre factors (Fig. 5, *B* and *C*). The fraction of U18 RNA corresponding to the third pause was plotted over time to perform kinetic analysis (Fig. 5, *B* and *C*). In the absence of Gre factors, pause escape was faster at alkaline pH, with an average pause dwell time of 130 s at pH 7.2 compared with 108 s at pH 8.5 (Fig. 5, *B* and *C*). About 22% of ECs entered the pause at pH 7.2 *versus* 11% at pH 8.5 (Fig. 5, *B* and *C*), suggesting that the third pause captured a greater fraction of ECs at neutral

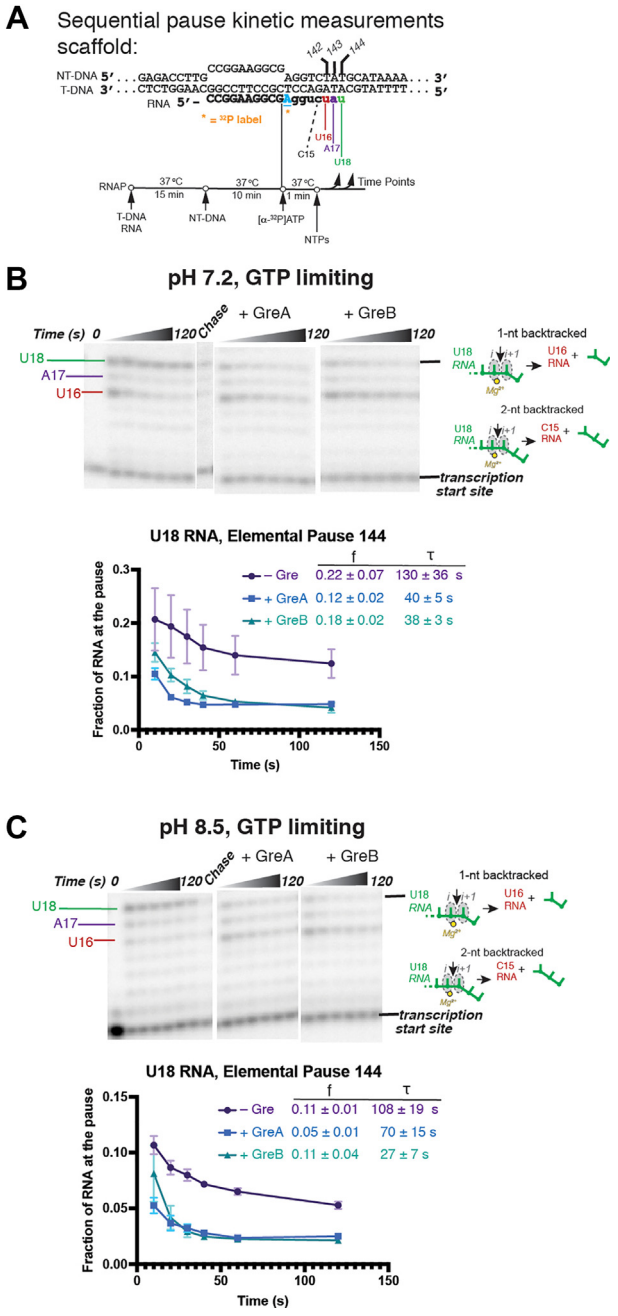

Figure 5. Measurement of pause kinetics at the third backtracked sequential pause during active transcription elongation in the presence and absence of Gre factors. *A*, experimental overview of sequential pause kinetic experiments. ECs were positioned upstream of the pauses on the nucleic acid scaffold shown. Transcription was initiated by addition of all four NTPs, with GTP present at a limiting concentration to increase the duration of the third pause. Time points were taken at regular intervals ranging from 0 s to 120 s. *B*, kinetic measurements for the third pause in the sequential series downstream of hairpin S. *Top panel*, representative gel images from transcription time courses performed at pH 7.2. U16, A17, and U18 RNAs correspond to the first, second, and third sequential pauses, respectively. *Cartoons* adjacent to the rightmost gel panel depict the proposed backtracked registers adopted by ECs at the third pause. "Chase" represents a sample taken after allowing elongation to proceed for 5 min with saturating NTP. *Bottom panel*, results from gel quantification of the U18 pause RNA fraction over time at pH 7.2 in the presence and absence of Gre factors. Error is SD of triplicate. The table adjacent to the plot reports the pause efficiencies (f) and average pause dwell times (τ). *C*, kinetic measurements for the third pause in the sequential series downstream of hairpin S. *Top panel*, representative gel images from transcription time courses performed at pH 8.5. U16, A17, and U18 RNAs correspond to the first, second, and third sequential pauses, respectively. *Cartoons* adjacent to the rightmost gel panel depict the proposed backtracked registers adopted by ECs at the third pause. "Chase" represents a sample taken after allowing elongation to proceed for 5 min with saturating NTP. *Bottom panel*, results from gel quantification of the U18 pause RNA fraction over time at pH 8.5 in the presence and absence of Gre factors. Error is SD of triplicate. The table adjacent to the plot reports the pause efficiencies (f) and average pause dwell times (τ). EC, elongation complex.

pH *versus* alkaline pH. These observations are consistent with the experiments positioning ECs directly at the third pause to measure the escape rate, where we observed an incomplete decay for the pause RNA fraction over time and a greater population of PECs that escaped the pause at alkaline pH *versus* neutral pH (Fig. 4*C*).

Upon addition of GreA, pause escape was slower at alkaline pH, with an average pause dwell time of 40 s at pH 7.2 and 70 s at pH 8.5 (Fig. 5, *B* and *C*). When GreB was present, pause escape was faster at alkaline pH, with an average pause dwell time of 38 s at pH 7.2 and 27 s at pH 8.5 (Fig. 5, *B* and *C*). On the whole, addition of either GreA or GreB decreased the average pause dwell time compared with the no-factor condition under both neutral and alkaline conditions, supporting that the Gre factors stimulated RNA cleavage to promote rescue of backtracked PECs. It is unclear why the pause lifetime increased at pH 8.5 in the presence of GreA yet decreased at pH 8.5 in the presence of GreB, since it is expected that alkaline pH would increase the rate of RNA cleavage *via* hydrolysis in general (19). While we did not observe a consistent trend between pH and pause lifetimes at the third pause, the effect of pH on pause efficiency was similar in the presence and absence of Gre factors. With GreA present in the transcription elongation assay, 12% of ECs entered the pause at neutral pH compared with 5% at alkaline pH (Fig. 5, *B* and *C*). When GreB was present, 18% of ECs entered the pause at neutral pH compared with 11% at alkaline pH (Fig. 5, *B* and *C*). We consistently observed that the pause efficiency was greater at neutral pH *versus* alkaline pH in the presence and absence of Gre factors, suggesting that a smaller population of ECs entered the third backtracked pause under alkaline pH during active transcription elongation. In addition, we observed a clear increase in the U16 RNA fraction upon addition of Gre factors (Fig. S5*A*) and a concomitant decrease in the U18 fraction, supporting that the U16 RNA results from Gre factor–stimulated cleavage of backtracked PECs. Thus, the cleavage event at the third pause repositions ECs at the first pause in the sequential series, increasing the flux of ECs through sequential pauses (see Supporting Discussion section for further analysis of the translocation register at the third pause during active elongation). Altogether, our data support that ECs at the third pause are backtracked, and this backtracking event occurs when ECs encounter the third pause during active transcription elongation, which holds potential relevance for PRE RNA folding.

Pause 142 analysis

To visualize the first pause and probe the effect of Gre factors on its longevity, we performed transcription elongation

assays at a limiting concentration of ATP (10 μM) (Fig. S5*B*). The fraction of U16 RNA corresponding to the first pause was plotted over time to perform kinetic analysis (Fig. S5*B*). In the absence of Gre factors, pause escape was slower at neutral pH, with an average pause dwell time of 45 s at pH 7.2 compared with 20 s at pH 8.5 (Fig. S5*B*). This trend is consistent with results from the transcription assay that positioned ECs directly at the first pause (Fig. 4*A*). About 55% of ECs entered the pause at pH 7.2 *versus* 27% at pH 8.5 (Fig. S5*B*), demonstrating that the first pause captured more ECs at neutral pH *versus* alkaline pH.

When either GreA or GreB was introduced in the limiting ATP condition, there was a marked increase in the U16 RNA fraction, resulting from a backtracking and Gre-catalyzed 2-nt or 3-nt cleavage at the third pause that repositioned the ECs at the first pause (Fig. S5*B*). The U16 RNA fraction became more prominent in this experiment because ATP, the incoming NTP at the first pause, was present at a limiting concentration. In the presence of GreA, pause escape was slower at neutral pH, with an average pause dwell time of 85 s at pH 7.2 compared with 29 s at pH 8.5 (Fig. S5*B*). In the presence of GreB, pause escape was also slower at neutral pH, with an average pause dwell time of 178 s at pH 7.2 compared with 53 s at pH 8.5 (Fig. S5*B*). Under both pH conditions, the average time spent by ECs at the first pause increased in the presence of Gre factors because of repopulation of ECs at the first pause following the cleavage event at the third backtracked pause. Specifically, in the presence of GreA, 63% of ECs entered the first pause at pH 7.2 compared with 40 % at pH 8.5 (Fig. S5*B*), exhibiting that the first pause captured more ECs at neutral pH *versus* alkaline pH. In the presence of GreB, 73% of ECs entered the first pause at pH 7.2 compared with 76% at pH 8.5 (Fig. S5*B*), demonstrating that the first pause captured a slightly greater fraction of ECs at alkaline pH *versus* neutral pH. Altogether, our analysis of the first sequential pause corroborates the kinetic results obtained at the third sequential pause: ECs at the third pause are backtracked and Gre factor–stimulated cleavage increases RNAP traffic through the sequential pauses. Furthermore, we consistently observed that pause escape is accelerated by alkaline pH when the first pause is encountered by ECs during active transcription elongation.

Pause 143 analysis

Finally, we performed transcription elongation assays at a limiting concentration of UTP (10 μM) to increase the duration of the second pause and evaluate the pause lifetime and efficiency at different pH. The fraction of A17 RNA corresponding to the second pause was plotted over time to perform kinetic analysis (Fig. S5*C*). In the absence of Gre factors, pause escape was faster at alkaline pH, with an average pause dwell time of 34 s at pH 7.2 and 30 s at pH 8.5 (Fig. S5*C*). About 18% of ECs entered the pause at pH 7.2 compared with 17% at pH 8.5 (Fig. S5*C*), demonstrating that the second pause captured a similar fraction of ECs at both pH.

When either GreA or GreB was introduced in the limiting UTP condition, there was a marked increase in both the U16 and A17 RNA fractions (Fig. S5*C*). The increase in the U16 and A17 RNA fractions was due to an increased flux of ECs through the first and second pauses following the backtracking and Gre-catalyzed 2–3-nt RNA cleavage at the third pause. The A17 RNA corresponding to the second pause became more prominent in this experiment since UTP, the incoming NTP at the second pause, was limiting. In general, the A17 RNA fraction did not increase to the same degree as the U16 RNA fraction upon addition of Gre factors. It appears that the second pause is weaker than the first pause and consequently captures fewer ECs that re-enter elongation following backtracking and cleavage at the third pause. Interestingly, we observed that the pause efficiencies were greater at alkaline pH *versus* neutral pH in the presence of Gre factors. Specifically, upon addition of GreA, 32% of ECs entered the pause at pH 7.2 *versus* 36% of ECs at pH 8.5 (Fig. S5*C*). In the presence of GreB, 26% of ECs entered the pause at pH 7.2 *versus* 47% of ECs at pH 8.5 (Fig. S5*C*). For the measured pause escape rates, the effect of pH was consistent with what was observed in the no-factor condition, with faster pause escape at alkaline pH. In the presence of GreA, pause escape was faster at alkaline pH, with an average pause dwell time of 26 s at pH 7.2 and 20 s at pH 8.5 (Fig. S5*C*). In the presence of GreB, pause escape was also faster at alkaline pH, with an average pause dwell time of 70 s at pH 7.2 and 34 s at pH 8.5 (Fig. S5*C*). Overall, our observations in these experiments remained consistent with the results outlined in prior sections, further supporting an increase in flux of ECs through the sequential pauses following Gre factor–assisted cleavage at the third pause. In addition, similar to our observations at the first pause, we consistently observed that pause escape is faster at alkaline pH when the second pause is encountered by ECs during active transcription elongation.

E. coli *RNAP pause longevity is decreased by alkaline pH at the second major pause site in the pH-responsive riboswitch folding pathway*

We next investigated how pH affects elemental pause escape kinetics at pause 2, the second critical decision point for PRE folding. To locate pause 2 and measure the pause lifetimes at different pH, we performed scaffold-based transcription assays in a similar fashion to our analysis of pause 1. Specifically, we reconstituted ECs on a synthetic DNA–RNA scaffold corresponding to position 173 on the PRE (G10 ECs)—upstream of the originally mapped pause 2 location at the PRE nt 182—and the G10 ECs were radiolabeled *via* incorporation of [α-^{32}P] ATP, extending the RNA to form A11 ECs (Fig. 6*A*). Transcription elongation was initiated upon addition of all four NTPs to the A11 ECs, with the incoming NTP corresponding to each pause present at a limiting concentration to increase pause duration and permit manual quenching. To obtain kinetic parameters, a semilogarithmic plot was generated for the pause RNA fraction over time and a single-exponential decay fitting was performed on the plot. In the original PRE folding model, it was proposed that pause 2, in addition to pause 1, is prolonged by alkaline pH to promote folding of

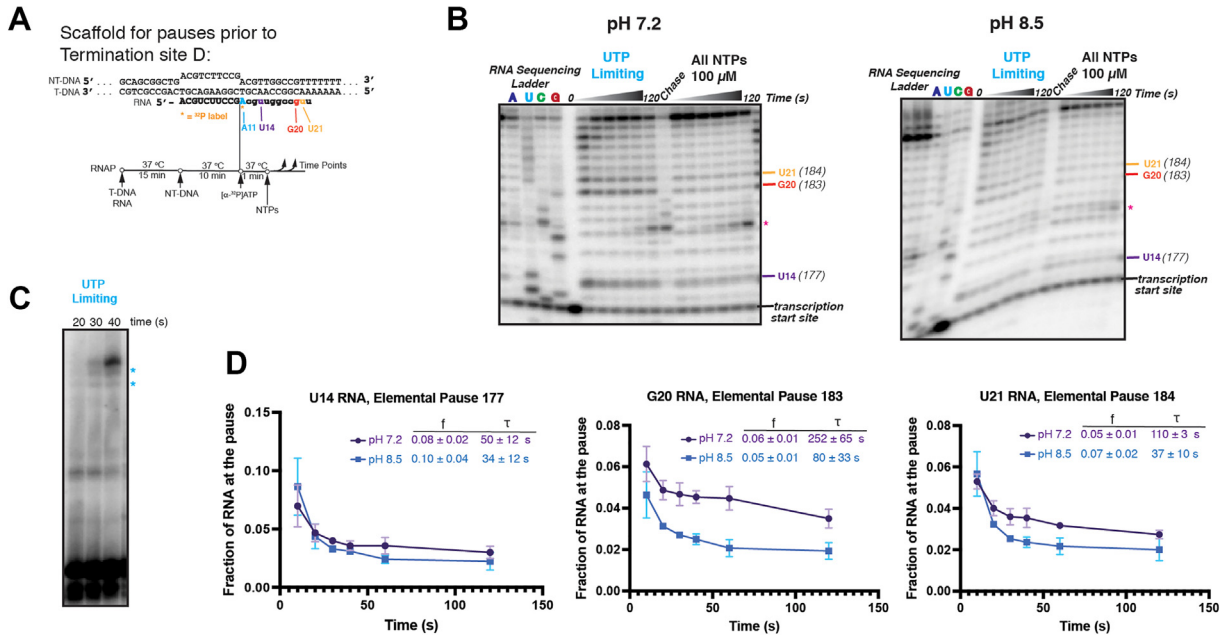

Figure 6. Measurement of pause kinetics at pause 2 during active transcription elongation. *A*, experimental overview of pause 2 mapping and pause escape kinetic experiments. ECs were positioned upstream of the pauses on the nucleic acid scaffold shown. Transcription was initiated by addition of all four NTPs. Time points were taken at regular intervals ranging from 0 s to 120 s. *B*, representative gel images from transcription time courses performed at pH 7.2 and 8.5. Time-course samples were run alongside an RNA sequencing ladder for precise mapping of pause locations. U14, G20, and U21 RNAs represent pauses that were enhanced in the UTP limiting condition and correspond to nt 177, 183, and 184 on the PRE, respectively. "Chase" represents a sample taken after allowing elongation to proceed for 5 min with saturating NTP. The band marked with an *asterisk* (*) of unknown origin accumulated at long reaction time and high NTP concentration. *C*, gel image of synchronized single-round *in vitro* transcription from the *alx* promoter conducted at a limiting concentration of UTP. The UTP limiting condition increased the duration of multiple pauses prior to termination site D, which are denoted with an *asterisk* (*). The image for the UTP limiting time course is the same image from Figure 3*D*. This image was reused here to iterate that the pauses observed under the UTP limiting condition in scaffold experiments are relevant in the context of the full-length RNA. *D*, results from gel quantification of the U14, G20, and U21 RNA fractions over time at pH 7.2 and 8.5. Error is SD of triplicate. The table adjacent to the plots report the pause efficiencies (f) and average pause dwell times (τ). EC, elongation complex; PRE, pH-responsive element.

hairpin C/D in the PRE active conformer (Figs. 1*B* and S1). Similar to our investigation of pause 1, we focused solely on elemental pause longevity and its response to pH since the elemental pause is a necessary precursor for longer-lived pauses that may mediate PRE folding.

We first performed this experiment limiting the concentration of GTP to test for pause 2, which was originally reported to reside at position 182 on the PRE sequence (2) (see Fig. S1 and Table S1 for PRE sequence). However, we did not find evidence for this pause location in our experiments (Fig. S6*A*), suggesting that pause 2 was mapped incorrectly. The reported location of pause 2 was likely incorrect because of limited resolution of the gel analysis of long RNAs produced from promoter-initiated transcription, similarly to pause 1 mapping. Nevertheless, multiple pauses were enhanced in the UTP limiting condition at both pH, indicating that these are most likely the relevant pauses prior to the termination site D (Fig. 6*B*). Consistent with this observation, in promoter-initiated transcription experiments, we observed increased pause longevity for the pauses prior to termination site D in the UTP limiting condition (Fig. 6*C*). We mapped these pauses to positions 177, 183, and 184 on the PRE sequence (Fig. 6*B*), placing them in the vicinity of the originally mapped pause 2 location. We compared these pause sequences to the consensus elemental pause sequence (Fig. S6*B*), which was identified in a prior NET-seq study (27). Overall, the pauses do not contain many sequence features in common with those most frequently observed *in vivo* in *E. coli*; however, the pause consensus results from genome-wide averaging, and it is not necessarily expected that all pauses will share sequence similarity with the consensus sequence. In addition, to assess whether the newly mapped pauses at positions 177, 183, and 184 occur *in vivo*, we analyzed the previously reported NET-seq data for the entire *E. coli* genome (27). From these data, we observed sequencing reads above baseline for position 177 but not for positions 183 and 184 (Fig. S6*C*). It is unclear why there is a discrepancy between our *in vitro* pause mapping data and the NET-seq results. Further experimentation will be required to confirm the locations of the pauses prior to termination site D *in vivo*.

With the pauses prior to termination site D mapped, we performed additional transcription elongation assays at a limiting concentration of UTP (10 μM) to increase the duration of each pause and evaluate the pause lifetimes and efficiencies at different pH (Table S4). The fractions of U14, G20, and U21 RNAs were plotted over time to perform kinetic analysis of the pauses at positions 177, 183, and 184, respectively (Fig. 6*D*). For the elemental pause at position 177, pause escape was faster at alkaline pH, with an average pause dwell time of 50 s at pH 7.2 and 34 s at pH 8.5 (Fig. 6*D*). At position 183, pause escape was also faster at alkaline pH, with an average pause dwell time of 252 s at pH 7.2 and 80 s at pH 8.5

(Fig. 6*D*). Finally, at position 184, the average pause dwell time was 110 s at pH 7.2 and 37 s at pH 8.5 (Fig. 6*D*), demonstrating faster pause escape at alkaline pH. Altogether, pause escape was faster at alkaline pH for each pause prior to the termination site D, which is consistent with our analysis from promoter-initiated transcription experiments where we also observed faster pause escape at alkaline pH (Fig. S2*C*).

Discussion

In this work, we investigated the proposed folding mechanism for the *E. coli* pH-responsive riboswitch. Previous study clearly supports that PRE folding is kinetically controlled *via* strategically located RNAP pause sites (2). This prior study reported promoter-initiated transcription experiments in which multiple pause sites were visualized at both neutral and alkaline pH (2). From these data, gel quantification of the pause RNA species was performed using the metric "half maximal intensity," and two pause species in particular were found to have greater half maximal intensity values for later time points at alkaline pH (2). This analysis led to the conclusion that alkaline pH enhances RNAP pausing at two sites to support PRE folding into the translationally active conformer. The method of gel quantification and reproducibility, however, were not specified, and the overall effect of alkalinity on the transcription rate was not considered. Thus, these previously reported observations did not discriminate between two potential mechanisms of pH action: pH rearranging paused RNAP structure to prolong its residence time at key pause sites *versus* pH acting directly on the RNA cotranscriptionally to promote its folding into the active conformer. Here, we performed a rigorous analysis of *E. coli* RNAP pausing kinetics under different pH conditions at the biologically relevant pauses for PRE folding and posit that the RNA plays a role in sensing the cytosolic pH.

We initially investigated the first major pause site in the PRE folding pathway, which was suggested to facilitate the folding of hairpin S, a key structural element in the active conformer thought to ultimately determine whether the RBS in the PRE is accessible (Fig. S1). We uncovered that the pause downstream of hairpin S was mapped incorrectly; instead, our pause mapping experiments demonstrated a series of three sequential pauses ∼4 nt downstream of the originally published site. This updated location is still consistent with pause 1 being a critical driver of PRE RNA folding, where point mutations within the pause sequence that changed either the duration or location of pause 1 altered *alx* gene expression (9). Specifically, the A132G mutation was found to significantly increase the duration of pause 1 relative to the wild-type PRE sequence, whereas the C135U and A137G substitutions shifted the location of pause 1 downstream from its original position (9). With the improved sequence location of pause 1, we can shed new insights into the observed effects of the mutations on pausing. The A132G mutation places a G in the −11 position at the first sequential pause, increasing its sequence similarity to the pause consensus and explaining the observed increase in pause 1 duration (Fig. S8). Since C135U and A137G were found to shift the location of pause 1 downstream of the original site, it is possible that the mutations increased the propensity of RNAP to pause at a location downstream of the wild-type sequence. For example, the A137G mutation creates a sequence motif with a high degree of similarity to the pause consensus shifted a few nt downstream of the sequential pauses (Fig. S8).

pH effect on the key pauses in the PRE folding pathway

Once mapped more precisely, we placed RNAP at the pause 1 sequential pauses and measured the elemental pause escape rate at neutral *versus* alkaline pH, thus testing whether alkaline pH acts directly on paused RNAP to drive the ultimate RNA folding outcome. We found that the elemental pause escape rate at these pauses is not increased by alkaline pH, demonstrating that alkaline pH does not alter paused RNAP structure directly to facilitate PRE folding into the active conformer. Further experiments to measure pause escape kinetics at the sequential pauses produced the following insights: (i) the third pause in the sequential series is backtracked and likely adopts the 1- to 2-nt backtracked registers when the pause is encountered during active transcription elongation; (ii) Gre factor–stimulated RNA cleavage at the third pause increases traffic through the sequential pauses, and (iii) in general, pause escape was faster at alkaline pH *versus* neutral pH across all pauses in the sequential series when encountered by ECs during active transcription elongation. In addition, in promoter-initiated transcription assays where the full-length PRE RNA is present, we observed that addition of GreA consolidated the multiple RNA bands constituting pause 1 and enhanced the duration of earlier pauses in the sequential series —confirming the relevance of our results from scaffold-based transcription experiments.

We also investigated the pH dependence of pause escape at pause 2, which was proposed to be prolonged by alkaline pH to promote the folding of hairpin C/D in the active conformer (Figs. 1*B* and S1). Similar to pause 1, we found that pause escape at pause 2 is accelerated by alkaline pH. Altogether, our results demonstrate that pH exerts an effect on paused RNAP independent of the nascent riboswitch RNA but not in the originally proposed manner. Instead, our data support that ECs spend more time on average at pauses 1 and 2 at *neutral pH*. Therefore, a new framework is required to explain the changes in PRE RNA structure that occur at different pH, as we propose in a later section.

Potential role of nascent RNA structure modulating pause longevities during PRE synthesis

While previous work suggested nascent RNA hairpin modulating pause 1 longevity (2), the newly mapped locations for pause 1 call this assertion into question. The most well-characterized pause class involving nascent RNA structure is the hairpin-stabilized pause, where the RNA hairpin is positioned ∼11 nt away from the RNA 3′ end at the active site of RNAP (Fig. S7*A*). The three sequential pauses we mapped downstream of hairpin S are 17 to 19 nt away from the RNA 3′

end, positioning hairpin S well outside the RNAP exit channel, even upon backtracking by 1 to 2 nt at the third pause; therefore, the sequential pauses are likely unaffected by the proposed hairpin S in the nascent RNA (Fig. S7*B*). In addition, hairpin S is not the only RNA structure forming in the vicinity of pause 1 since hairpin C, which forms in the inactive conformer, also nucleates in proximity of pause 1 (Fig. S1). In contrast to hairpin S, which is spaced too far from the RNAP exit channel to promote a hairpin-stabilized pause, hairpin C can only begin nucleation after ECs have bypassed pause 1 (Fig. S7*C*).

Although it appears unlikely that either hairpin S or hairpin C modulate pause 1 longevity, an interplay between the nascent PRE RNA and pausing cannot be ruled out. Our test for hairpin-stabilized pauses in the region critical for pH-responsive riboswitching yielded inconclusive results. Specifically, NusA significantly enhanced termination at site B and decreased the flux of ECs through pauses 1 and 2, preventing a definitive conclusion as to whether hairpin-stabilized pauses exist at these locations. At this point, we can only consider the influence of RNA structural motifs present in the fully folded RNA on the pauses, which further limits our analysis. It is possible that the PRE traverses through transient structures that have not yet been characterized. For example, we observed multiple pauses enhanced by NusA prior to the termination site B that could not be rationalized in the context of the full-length RNA secondary structure models. Thus, a necessary aim of future work will be to map RNA structural intermediates with newly developed approaches such as cotranscriptional SHAPE-seq (35). It is also possible that a more complex RNA structural motif modulates pause longevity in the vicinity of the sequential pauses, which could not be captured in our experiments. We currently lack detailed three-dimensional structural information for the PRE RNA, which further limits investigation into a potential interplay between the nascent RNA structure and pausing. Recently, a novel pause stabilized by an RNA pseudoknot was identified for the preQ$_1$ riboswitch, highlighting a cross-coupling between riboswitch folding and RNAP pausing (36). By analogy to preQ$_1$ riboswitch, it is possible that a complex RNA structural motif modulates pause longevity at the sequential pauses within the PRE. Additional experiments that report on both local and global RNA structure will be required to investigate how the pH-responsive riboswitch folds cotranscriptionally in general and the specific RNA structural motifs proximal to RNAP at the sequential pauses.

To assess the effect of alkaline pH on a classical pause stabilized by nascent RNA structure, we investigated the pH dependence of RNAP pause escape kinetics at the *his* pause—a well-characterized hairpin-stabilized pause that has served as an important model system to advance our understanding of hairpin-stabilized pauses (11). We performed scaffold-based experiments to characterize RNAP pause escape kinetics at the *his* pause under neutral and alkaline conditions both in the presence and absence of NusA (Fig. S7*D*). We observed that pause escape was faster at pH 8.5 compared with pH 7.2 both in the presence and absence of NusA (Fig. S7*E*), consistent with our results testing the pH dependence of the elemental pauses relevant to PRE folding. Therefore, if a nascent RNA hairpin that modulates pause 1 longevity was missed in the scope of our experiments, it is unlikely that the pause duration is enhanced by alkaline pH either in the presence or in the absence of NusA.

An alternative model for pH-dependent PRE folding

Since we observed that ECs transcribe through the PRE sequence faster at alkaline pH, one possibility is that a faster transcription rate alone is required for formation of the translationally active PRE conformer. However, this explanation is inconsistent with the prior observation that *in vitro* synthesis of the PRE by T7 RNAP at alkaline pH does not shift the RNA ensemble to the active conformer (2). Thus, the faster transcription rate at alkaline pH is insufficient to explain the RNA structural switch. Since T7 RNAP pauses less than *E. coli* RNAP (10), this observation supports that pauses during PRE synthesis are strategically located to guide the RNA folding. Pauses in other riboswitch folding pathways have been found to guide proper folding decisions and can provide a time window for ligand binding (26, 36, 37), so it is possible that the pauses in the PRE folding pathway fit this paradigm and provide a time window for alkaline pH to act on the RNA. Also, it is intriguing that three sequential pauses were uncovered in our experiments. Sequential pauses have been observed in leader regions that regulate *Bacillus subtilis* gene expression (38, 39) and were also found throughout the *B. subtilis* genome in an RNET-seq study (40). It is currently unclear what functional role sequential pauses play in the context of the PRE. Altogether, while we conclude that both pause 1 and pause 2 do not display the kinetics proposed in prior work, they are likely important to the ultimate RNA folding outcome at different pH.

An alternative model for PRE folding that unifies our observations with prior work is a model with elements of *both* kinetic control and a direct effect of pH on the RNA. We propose that pausing provides a temporal window for pH to exert an effect on the RNA structure and guide the biologically functional outcomes. Since the PRE alters its cotranscriptionally folded structure upon a shift from neutral to alkaline pH, it is possible that a nucleobase deprotonation event triggers the structural switch at alkaline pH. Typically, unmodified nucleosides in RNA are expected to be neutrally charged at biological pH, since the pK_a values closest to neutrality in RNA nucleobases are 3.5 for N1 of adenosine, 4.2 for N3 of cytidine, and 9.2 for both N1 of guanosine and N3 of uridine (41). However, the structural environment in a folded RNA can shift these pK_a values significantly toward neutrality (42–46). There are many examples where upwardly shifted pK_as of A or C residues in an RNA result in protonation under physiological conditions, which in turn modulates the RNA structural ensemble. For example, protonation of a C in a C$^+$•G-C base triple (pK_a = 6.8) in the beet western yellow virus mRNA was found to stabilize an RNA pseudoknot critical for translational frameshifting (42). Protonation of an A with a pK_a of 6.23 in

the murine leukemia virus mRNA tunes the conformational equilibria to control the level of translational frameshifting (43). Examples of functionally relevant protonation events span beyond viruses and have been characterized for the U6 spliceosomal RNA (44), a bacterial group II intron (45), and a microRNA (46). The most commonly protonated base pairs are A^+-C and C^+-C (47), and while the PRE structural models lack such base pairs as they currently stand, many of the RNA examples outlined previously highlight the potential for more complex effects of base protonation/deprotonation events on RNA structural motifs beyond simple base pairing. Furthermore, functionally relevant protonation events for both the bacterial group II intron and microRNA noted previously involve a protonated A^+-G base pair, further expanding the scope of possibilities for pH sensing in the PRE. Finally, a quantum chemical study that surveyed available RNA crystal structures identified eight base pairs that can exist in both protonated and nonprotonated geometries and could act as pH-dependent switches (48). This study also identified a wide range of higher order RNA structural interactions where protonation likely plays a stabilizing role (48). Thus, it is possible that a deprotonation event destabilizes a particular tertiary structural element of PRE at alkaline pH, altering the energetics underlying the RNA folding and shifting the RNA ensemble toward the translationally active conformer. We currently lack detailed three-dimensional structural information for the PRE, which will be an essential aim of future work to identify specific putative protonation sites that may mediate a conformational switch. More broadly, a complete mechanistic picture for the pH-responsive riboswitch will provide important insights for the development of pH-tuned genetic control elements.

Experimental procedures

Reagents and materials

All plasmids and oligonucleotides used in this study are listed in Table S1. Synthetic construct encoding wild-type PRE (nt 1–207) under control of its native *alx* promoter was purchased in pUC57-Kan vector from Bio Basic. All RNA and DNA oligos for transcription experiments were obtained from Integrated DNA Technologies. RNAs were purified before use by denaturing PAGE through 15% gels (19:1 acrylamide:bisacrylamide) with 8 M urea and 89 mM Tris base, pH 8.3, 89 mM boric acid, and 2 mM EDTA buffer. Full-length RNAs were visualized with UV shadowing, excised, and incubated overnight in low salt oligo purification buffer (10 mM Tris–Cl, pH 7.5, 1 mM EDTA, and 100 mM NaCl). The gel-extracted RNAs were applied to DEAE Sepharose resin (Cytiva), eluted with a high salt oligo purification buffer (10 mM Tris–Cl, pH 7.5, 1 mM EDTA, and 2 M NaCl), and ethanol precipitated. Linear double-stranded DNA templates for promoter-initiated *in vitro* transcription were prepared by PCR with high-fidelity Q5 DNA polymerase (New England Biolabs), treated with DpnI (New England Biolabs), and purified by phenol/chloroform extraction followed by ethanol precipitation prior to use. Primers for the PCR were from Integrated DNA Technologies. Initiating dinucleotide for promoter-initiated transcription (GpC) and 3′-deoxynucleotides for RNA sequencing ladder were from TriLink BioTechnologies. NTPs for transcription experiments were purchased as HPLC purified from Cytiva. ^{32}P-labeled NTPs were from PerkinElmer.

Preparation of E. coli RNAP and σ^{70}

E. coli RNAP was prepared as follows. BL21(DE3) cells were transformed with pRM756 (obtained from the Landick laboratory, University of Wisconsin-Madison), an overexpression plasmid for wild-type *E. coli* RNAP with a PreScission Protease–cleavable His_{10} tag on the C terminus of the β′ subunit. Cells were grown in 3× 1 l Luria broth on a 37 °C shaker (200 rpm) to an absorbance of 0.25 at 600 nm. The temperature was dropped to 16 °C, and cultures continued to grow with shaking (200 rpm) to an absorbance of 0.4 at 600 nm. Cultures were induced with 1 mM IPTG and grown overnight with shaking (200 rpm) at 16 °C. Cells were pelleted by centrifugation at 4 °C (4000 rpm). The cell pellet was resuspended in 30 ml of lysis buffer (50 mM Tris–Cl, pH 7.9, 5% glycerol, 233 mM NaCl, 2 mM EDTA, 10 mM 2-mercaptoethanol, 10 mM DTT, and protease inhibitor cocktail [Sigma–Aldrich]) per 2 l of culture and sonicated for a total of 30 min (20 s on/20 s off, amplitude 60%) at 4 °C. All subsequent purification steps were carried out at 4 °C. The lysate was spun at 11,000*g* for 15 min. Cleared supernatant was subjected to polyethyleneimine precipitation by slow addition of polyethyleneimine to 0.6% v/v with gentle stirring. After stirring for 10 min, the precipitate was recovered by centrifugation at 11,000*g* for 15 min. The pellet was resuspended in TGEDZ buffer (10 mM Tris–Cl, pH 7.9, 5% glycerol, 0.1 mM EDTA, 5 μM $ZnCl_2$) + 0.5 M NaCl to salt-in unwanted proteins, and the suspension was centrifuged at 11,000*g* for 15 min. The pellet was resuspended in TGEDZ buffer + 1 M NaCl to salt-in RNAP, and the suspension was centrifuged at 11,000*g* for 15 min. The supernatant was removed and subjected to ammonium sulfate precipitation. Ammonium sulfate was added to a final concentration of 0.37 g/l, and the solution was left stirring overnight. The solution was centrifuged at 27,000*g* for 15 min. The pellet was resuspended in HisTrap buffer A (20 mM Tris–Cl, pH 7.9, 500 mM NaCl, 5 mM imidazole, and 5 mM 2-mercaptoethanol), filtered with a 0.2 μM filter to remove particulates, and applied to a GE HisTrap HP 5 ml column. RNAP was eluted over 10 column volumes with a gradient of 5–250 mM imidazole. Fractions containing RNAP were identified *via* SDS-PAGE and pooled. The NaCl concentration in the pooled fractions was reduced to 200 mM with addition of TGEDZ buffer. Pooled fractions were then loaded onto a GE HiTrap Heparin HP 5 ml column to compete nucleic acids off of RNAP. RNAP was eluted *via* a step elution by increasing the NaCl concentration from 200 mM to 500 mM. Fractions containing RNAP were identified *via* SDS-PAGE, pooled, and concentrated to a final volume of 2 ml with an Amicon Ultra Centrifugal Filter (100 kDa molecular weight cutoff). The concentrate was loaded into

a dialysis cassette (Thermo Fisher Scientific) and dialyzed into storage buffer (10 mM Tri–Cl, pH 7.9, 25% glycerol, 100 mM NaCl, 100 μM EDTA, 1 mM $MgCl_2$, 20 μM $ZnCl_2$, and 10 mM DTT) with stirring overnight. Small aliquots of purified RNAP were transferred into microcentrifuge tubes and stored at −80 °C until use.

Wild-type *E. coli* σ^{70} was prepared as follows. T7 Express cells were transformed with pMIS4 (originally obtained from the Burgess laboratory, University of Wisconsin-Madison), an overexpression plasmid for wild-type *E. coli* σ^{70} with an N-terminal His_6 tag. Cultures were grown on a shaker (200 rpm) at 37 °C to an absorbance of 0.5 at 600 nm and induced by addition of IPTG to 0.4 mM. The temperature was dropped to 16 °C, and cells were grown with shaking (200 rpm) overnight. Cells were harvested by centrifugation at 3000*g* for 15 min at 4 °C. All subsequent purification steps were carried out at 4 °C. The cell pellet was resuspended in lysis buffer (50 mM Tris–Cl, pH 7.9, 5 mM imidazole, 5% glycerol, 233 mM NaCl, 2 mM EDTA, 10 mM 2-mercaptoethanol, and protease inhibitor cocktail). The cells were lysed *via* sonication. The lysate was centrifuged at 11,000*g* for 15 min. The cleared supernatant was filtered and applied to a GE HisTrap HP 5 ml column. σ^{70} was eluted over six column volumes *via* a two-step elution: the first step was performed over three column volumes at 300 mM imidazole, and the second step was performed over three column volumes at 500 mM imidazole. The fractions containing σ^{70} were identified *via* SDS-PAGE and pooled. The pooled fractions were run on a HiLoad 16/60 Superdex 200 preparative grade size exclusion column (Cytiva). The fractions containing σ^{70} were identified *via* SDS-PAGE and pooled. The pooled fractions were dialyzed overnight into a storage buffer (50 mM Tris, pH 7.9, 250 mM NaCl, and 30% glycerol). Small aliquots of purified σ^{70} were transferred into microcentrifuge tubes and stored at −80 °C.

Preparation of NusA, GreA, and GreB

NusA was prepared as follows. BL21(DE3) cells were transformed with pRA46, an overexpression plasmid for wild-type NusA with a His_6 tag on its N terminus. Cultures were grown on a shaker (200 rpm) at 37 °C to an absorbance of 0.5 at 600 nm and induced by addition of IPTG to 1 mM. The temperature was dropped to 16 °C, and cells were grown with shaking (200 rpm) overnight. Cells were harvested by centrifugation at 5000 rpm for 15 min at 4 °C. All subsequent purification steps were carried out at 4 °C. The cell pellet was resuspended in lysis buffer (50 mM Tris–Cl, pH 8.0, 10 mM imidazole, 500 mM NaCl, 2 mM 2-mercaptoethanol, 0.1 mM PMSF, 1 mM benzamidine, 2 μg/ml DNAse I, and protease inhibitor cocktail). The cells were lysed *via* sonication. The lysate was centrifuged at 13,000*g* for 30 min. The cleared supernatant was applied to a GE HisTrap HP 5 ml column. NusA was eluted *via* a step elution over six column volumes with 500 mM imidazole. The fractions containing NusA were identified *via* SDS-PAGE and pooled. The pooled fractions were run on a HiLoad 16/60 Superdex 200 preparative grade size exclusion column. The fractions containing NusA were identified *via* SDS-PAGE and pooled. The pooled fractions were dialyzed overnight into a storage buffer (20 mM Tris, pH 8.0, 200 mM NaCl, 1 mM EDTA, 1 mM DTT, 30% glycerol, and 0.1% Triton X-100). Small aliquots of purified NusA were transferred intro microcentrifuge tubes, flash frozen, and stored at −80 °C.

GreB was prepared as follows. BL21(DE3) cells were transformed with pIA577 (obtained from the Landick laboratory), an overexpression plasmid for wild-type GreB with a His_6 tag on its C terminus. Cultures were grown on a shaker (200 rpm) at 37 °C to an absorbance of 0.5 at 600 nm and induced by addition of IPTG to 1 mM. The temperature was dropped to 16 °C, and cells were grown with shaking (200 rpm) overnight. Cells were harvested by centrifugation at 5000 rpm for 15 min at 4 °C. All subsequent purification steps were carried out at 4 °C. The cell pellet was resuspended in lysis buffer (50 mM $NaPO_4$, pH 8.0, 5 mM imidazole, 10% glycerol, 250 mM NaCl, and protease inhibitor cocktail). The cells were lysed *via* sonication. The lysate was centrifuged at 11,000*g* for 15 min. The cleared supernatant was filtered and applied to a GE HisTrap HP 5 ml column. GreB was eluted over seven column volumes with a gradient of 25 to 300 mM imidazole. The fractions containing GreB were identified *via* SDS-PAGE and pooled. The pooled fractions were dialyzed overnight into a storage buffer (10 mM Tris–Cl, pH 8.0, 50% glycerol, 0.1 mM EDTA, 250 mM NaCl, and 2 mM DTT). Small aliquots of purified GreB were transferred into microcentrifuge tubes and stored at −80 °C.

GreA was prepared as follows. BL21(DE3) cells were transformed with pIA578 (obtained from the Landick laboratory), an overexpression plasmid for wild-type GreA with a His_6 tag on its C terminus. Cultures were grown on a shaker (200 rpm) at 37 °C to an absorbance of 0.5 at 600 nm and induced by addition of IPTG to 1 mM. The temperature was dropped to 16 °C, and cells were grown with shaking (200 rpm) overnight. Cells were harvested by centrifugation at 5000 rpm for 15 min at 4 °C. All subsequent purification steps were carried out at 4 °C. The cell pellet was resuspended in lysis buffer (100 mM Tris–Cl, pH 8.0, 100 mM NaCl, 10 mM EDTA, 40 μM PMSF, and 3 mg/ml lysozyme). The cells were lysed *via* sonication. The lysate was centrifuged at 11,000*g* for 15 min. The cleared supernatant was filtered and applied to a GE HisTrap HP 5 ml column. GreA was eluted over seven column volumes with a gradient of 25 to 300 mM imidazole. The fractions containing GreA were identified *via* SDS-PAGE and pooled. The pooled fractions were dialyzed overnight into a storage buffer (10 mM Tris–Cl, pH 8.0, 50% glycerol, 0.1 mM EDTA, 250 mM NaCl, and 2 mM DTT). Small aliquots of purified GreA were transferred into microcentrifuge tubes and stored at −80 °C.

Synchronized single-round in vitro *transcription from a promoter*

To monitor transcription on the PRE sequence when initiated from the *alx* promoter, we performed synchronized single-round *in vitro* transcription assays. The DNA template

for the *in vitro* transcription reactions was prepared *via* PCR using pMIS301 as a plasmid template. The transcription template contains the *alx* promoter, full PRE sequence, and a portion of the downstream gene (nt 1–59) termed *alx'*. Both the oligos and plasmid used for DNA template preparation are outlined in Table S1.

To prepare the RNAP holoenzyme, *E. coli* RNAP (2 μM) and σ^{70} (4 μM) were combined in transcription buffer (20 mM Tris–Cl, pH 7.2 or 8.5, 150 mM KCl, 10 mM $MgCl_2$, and 2.77 mM DTT) and incubated for 30 min at 37 °C. Following holoRNAP assembly, *in vitro* transcription reactions were initiated and synchronized, taking advantage of the natural lack of cytosines between positions 4 and 15 of the PRE. The initiation mix for *in vitro* transcription thus lacked CTP and contained 0.1 μM of the holoRNAP, 0.08 μM of the DNA template, 150 μM GpC dinucleotide, 25 μM UTP, 25 μM GTP, 10 μM ATP, [α-^{32}P]ATP, and transcription buffer at the appropriate pH. After allowing initiation to proceed for 15 min at 37 °C, rifampicin (Fisher) was added to a final concentration of 10 μg/ml, to inhibit reinitiation. Completion of this step yielded ECs stalled at the A15 position on the PRE.

Next, transcription elongation reactions were performed by combining 7.5 μl of ECs with 2.5 μl of an NTP mix containing 1 mM each ATP, UTP, CTP, and GTP (250 μM final, each NTP). All elongation reactions were performed at 37 °C. The final concentration of all NTPs in the transcription reactions was chosen to match the conditions used by Nechooshtan *et al.* (2). Transcription factors were introduced concurrently with NTPs to test their effect on transcription elongation and pausing. Specifically, to test the effect of NusA on transcription elongation, NTP mixes were prepared following the recipe outlined previously, and NusA was included at concentrations of 200 nM, 400 nM, 1 μM, and 2 μM such that its final concentrations were 50, 100, 250, and 500 nM in the experiment. To test the effect of GreA on transcription elongation, an NTP mix was prepared following the recipe outlined previously and GreA was included at a concentration of 2 μM such that its final concentration was 500 nM in the experiment. After beginning elongation, the reaction was quenched at desired time points with an equal volume of 2× stop buffer (90 mM Tris–borate buffer, 8 M urea, 50 mM EDTA, and 0.02% of both xylene cyanol and bromophenol blue). The time points collected were 4 s, 6 s, 8 s, 10 s, 12 s, 14 s, 20 s, 30 s, 45 s, 1 min, 1.5 min, and 2 min. In addition, chase reactions were performed at both pH 7.2 and 8.5 with each NTP present at a final concentration of 500 μM. Radiolabeled RNAs in the quenched samples were denatured for 2 min at 95 °C and separated using denaturing PAGE (10% 19:1 acrylamide:bisacrylamide, 8 M urea). Samples were run alongside a radiolabeled ladder (MspI-digested pBR322 plasmid). The gel was exposed to a PhosphorImager screen, and the screen was scanned using a Typhoon PhosphorImager.

Pause mapping using synchronized single-round in vitro *transcription from a promoter*

To better visualize the sequential pauses on the PRE when initiating transcription from the *alx* promoter, a similar protocol was used to the one described previously with a few modifications. The transcription buffer contained 20 mM Tris–Cl, pH 8.5, 150 mM KCl, 5 mM $MgCl_2$, and 5 mM DTT. The NTP concentrations used for the transcription reactions were lowered to slow pause escape and thus better visualize pause RNA species on denaturing PAGE gels. First, a set of transcription elongation reactions was performed with ATP, UTP, CTP, and GTP at a final concentration of 100 μM. The reactions were quenched at 5, 10, 20, and 30 s. Additional transcription elongation reactions were executed with one NTP limiting to extend the lifetime of each sequential pause. Specifically, three sets of reactions were performed with either ATP, UTP, or GTP limiting at a concentration of 20 μM, with the other three NTPs at a concentration of 100 μM. The reactions were quenched at 10, 20, 30, and 40 s. In parallel with the transcription elongation reactions, RNA sequencing ladders were generated to map the pauses prior to termination site B. The ECs were combined with ATP, UTP, CTP, and GTP to 100 μM and one 3′-deoxyNTP (TriLink BioTechnologies) to 500 μM. The sequencing reactions proceeded for 20 min at 37 °C and were quenched with an equal volume of 2× stop buffer. All sequencing reactions were performed at pH 8.5. Radiolabeled RNA in the quenched samples was heat-denatured for 2 min at 95 °C and separated using denaturing PAGE (10% 19:1 acrylamide:bisacrylamide, 8 M urea). Samples were run alongside a radiolabeled pBR322 ladder. A 10% denaturing PAGE gel was chosen to best resolve the sequential pause RNA species.

Pause mapping using scaffold-based transcription

To precisely map the pauses downstream of hairpin S in the PRE, a transcription elongation assay using a nucleic acid scaffold was performed. The nucleic acid scaffold initiated transcription upstream of the sequence window where pauses were expected to occur. PAGE-purified 19-mer RNA was 5′-^{32}P labeled. The labeling reaction contained 20 μM RNA, T4 Polynucleotide Kinase (PNK; New England Biolabs), [γ-^{32}P]ATP, 100 μM ATP, and 1× PNK buffer. PNK was then heat-inactivated for 3 min at 95 °C, and the 5′-^{32}P labeled RNA was purified with an Illustra Microspin G50 column (Cytiva) to remove unincorporated ATP. The nucleic acid scaffold was annealed in transcription buffer (20 mM Tris–Cl, pH 8.2, and 150 mM KCl), with 5 μM 5′-^{32}P labeled RNA and 10 μM T-DNA.

To reconstitute ECs, RNAP was combined with the nucleic acid scaffold in transcription buffer and incubated for 15 min at 37 °C, then the nontemplate DNA (NT-DNA) was added and incubation continued for an additional 10 min at 37 °C. The ratio of RNA:T-DNA:NT-DNA:RNAP was 1:2:5:3, corresponding to concentrations of 0.5, 1, 2.5, and 1.5 μM, respectively. Next, the ECs were diluted twofold in transcription buffer and applied to G50 resin to remove unbound scaffold. Heparin (Fisher) was added to the ECs at a final concentration of 0.1 mg/ml to bind any free RNAP. ECs were incubated with heparin for 3 min at 37 °C before starting transcription elongation reactions. Reactions were initiated by

adding ATP, UTP, CTP, and GTP to a final concentration of 100 μM, each. To increase pause duration, additional reactions were performed with either ATP, UTP, or GTP limiting at a concentration of 10 μM, with the other three NTPs at a concentration of 100 μM. $MgCl_2$ was added to a final concentration of 5 mM alongside NTP introduction. Samples were removed at time points ranging from 10 s to 80 s and quenched with an equal volume of 2× stop buffer. All remaining active ECs were chased off of the DNA scaffold by incubation with NTPs to a final concentration of 1 mM for 5 min at 37 °C.

In parallel with the transcription elongation reactions, RNA sequencing ladders were generated for precise mapping of pause locations. The ECs were prepared as described previously. The ECs were combined with ATP, UTP, CTP, and GTP to 100 μM and one 3′-deoxyNTP (TriLink BioTechnologies) to 1 mM. The sequencing reactions proceeded for 20 min at 37 °C and were quenched with an equal volume of 2× stop buffer. All sequencing reactions were performed at pH 8.2.

Radiolabeled RNAs from both the quenched time points and sequencing reactions were heat-denatured for 2 min at 95 °C and separated using denaturing PAGE (15% 19:1 acrylamide:bisacrylamide, 8 M urea). The gel was exposed to a PhosphorImager screen, and the screen was scanned using a Typhoon PhosphorImager.

Sequential pause escape kinetics positioning RNAP directly at the pauses

To measure the pause escape rate at each of the sequential pauses, PAGE-purified 17-mer RNA was 5′-^{32}P labeled using the same protocol implemented for the pause mapping assays (see above). The nucleic acid scaffolds for each pause in the sequential series (positions 142–144 on the PRE sequence) were annealed in a buffer (20 mM Tris, pH 7.2, and 150 mM KCl), with 5 μM 5′-^{32}P labeled RNA and 10 μM T-DNA. The T-DNA and NT-DNA used for these experiments included additional downstream DNA sequence compared with the DNA oligos used for pause mapping experiments to ensure that lost RNAP–DNA contacts because of shortening downstream DNA during transcription would not introduce artifacts into the measurements of pause lifetime.

To reconstitute ECs at the first pause, RNAP was combined with the nucleic acid scaffold in transcription buffer (20 mM Tris–Cl, pH 7.2 or 8.5, 150 mM KCl, 5 mM $MgCl_2$, and 5 mM DTT) and incubated for 15 min at 37 °C, then the NT-DNA was added, and incubation continued for 10 min at 37 °C. The ratio of RNA:T-DNA:NT-DNA:RNAP was 1:2:3:3, corresponding to concentrations of 0.5, 1, 1.5, and 1.5 μM, respectively. To reconstitute ECs at the second and third pauses, the same recipe as aforementioned was used but with Mg^{2+} omitted, to prevent intrinsic cleavage at the RNA 3′ end prior to initiating transcription. Next, the ECs were diluted twofold in transcription buffer and applied to an Illustra Microspin G50 column (Cytiva) to remove unbound scaffold. Heparin was added to the ECs at a final concentration of 0.1 mg/ml to sequester free RNAP. ECs were incubated with heparin for 3 min at 37 °C before starting the transcription reactions.

For the first pause in the sequential series, ATP was added to the PECs at a final concentration of 10 μM. Samples were removed at various time points and quenched with an equal volume of 2× stop buffer. All remaining active PECs were chased by incubation with ATP to a final concentration of 500 μM for 5 min at 37 °C.

For the second pause in the sequential series, UTP was added to the PECs at a final concentration of 10 μM. $MgCl_2$ was added to a final concentration of 5 mM alongside NTP introduction. Samples were removed at various time points and quenched with an equal volume of 2× stop buffer. All remaining active PECs were chased by incubation with UTP to a final concentration of 500 μM for 5 min at 37 °C.

For the third pause in the sequential series, GTP was added to the PECs at a final concentration of 20 μM. $MgCl_2$ was added to a final concentration of 5 mM alongside NTP introduction. Samples were removed at various time points and quenched with an equal volume of 2× stop buffer. All remaining active PECs were chased to product by incubation with GTP to a final concentration of 500 μM for 5 min at 37 °C.

Radiolabeled RNAs from the quenched time points were heat-denatured for 2 min at 95 °C and separated using denaturing PAGE (15% 19:1 acrylamide:bisacrylamide, 8 M urea was used for first and third pause in the sequential series, 20% 19:1 acrylamide:bisacrylamide, 8 M urea was used for the second pause in the sequential series). The gel was exposed to a PhosphorImager screen, and the screen was scanned using a Typhoon PhosphorImager. The gel images were quantified using ImageQuant software (GE Healthcare). For measurement of pause lifetimes, the average fraction of RNA at the pause was quantified for each time point. All measurements of the average pause RNA fraction report the average and standard deviation of time points performed in triplicate.

In addition to the sequential pause escape rate measurements, the pause 1 location reported by Nechooshtan *et al.* (2) (nt 138 on the PRE sequence) was tested with a scaffold-based transcription assay. The general protocol was the same as that used for the sequential pauses described previously. The experiments were conducted at pH 7.2 and 8.2 to match the conditions used in the original analysis of the PRE pauses (2). The nucleic acid scaffold used did not preserve the −11 position of the putative pause. In the wild-type PRE sequence, there is a C at the −11 position in the NT-DNA; the NT-DNA in our experiments had a T at this position instead. However, based on published work probing the contribution of the −11 position to overall pause strength, this substitution would only weaken the pause signal, not abolish it altogether as observed in our experiment (Fig. S3*A*) (28).

Testing for a backtracked register with ECs positioned at pause 144

To test for a backtracked register at the third pause, ECs were reconstituted directly at the pause following the same

protocol outlined previously to measure the GMP incorporation rate at different pH. ECs were reconstituted at both pH 7.2 and 8.5 in the presence or the absence of 5 mM $MgCl_2$. Following reconstitution, ECs for each pH and Mg^{2+} condition were incubated for 10 min at 37 °C in the presence or the absence of 1 μM GreA or GreB. The reactions were quenched with an equal volume of 2× stop buffer. Radiolabeled RNAs from the quenched samples were heat-denatured for 2 min at 95 °C and separated using denaturing PAGE (15% 19:1 acrylamide:bisacrylamide, 8 M urea). The gel was exposed to a PhosphorImager screen, and the screen was scanned using a Typhoon PhosphorImager. The gel image was quantified using ImageQuant software (Cytiva).

Sequential pause kinetics initiating transcription upstream of the pauses

To further investigate the pause escape kinetics at the sequential pauses, a scaffold-based transcription elongation assay was designed to initiate transcription elongation upstream of the sequential pauses. A 10-mer RNA was used to position RNAP upstream of the sequential pauses, with the 3′ G in the RNA corresponding to position 136 on the PRE sequence. The nucleic acid scaffold was annealed in a buffer (20 mM Tris, pH 7.2, and 150 mM KCl), with 5 μM RNA and 10 μM T-DNA. To reconstitute the G10 ECs, RNAP was combined with the nucleic acid scaffold in transcription buffer (20 mM Tris, pH 7.2 or 8.5, 150 mM KCl, and 5 mM DTT) and incubated for 15 min at 37 °C, then the NT-DNA was added, and incubation continued for 10 min at 37 °C. The ratio of RNA:T-DNA:NT-DNA:RNAP was 1:2:5:3 corresponding to concentrations of 0.5, 1, 2.5, 1.5 μM, respectively. Next, the ECs were diluted fivefold, and heparin was added to the ECs at a final concentration of 0.1 mg/ml to sequester free RNAP. ECs were incubated with heparin for 3 min at 37 °C. To radiolabel the ECs, [α-^{32}P]ATP was added to the ECs for 1 min at 37 °C, which extended the RNAs by 1 nt to form A11 ECs. To extend all ECs to A11, ECs were incubated with ATP at a final concentration of 2 μM for 3 min at 37 °C.

Multiple sets of transcription elongation reactions were performed to increase the duration of each pause in the sequential series and test the effects of GreA and GreB on pause escape at different pH. For all reactions, $MgCl_2$ was introduced at a concentration of 5 mM alongside the incoming NTPs. To assess the effect of pH and Gre factors on pause escape kinetics at each sequential pause, either ATP, UTP, or GTP was added at limiting concentrations of 10, 10, and 20 μM, respectively. All other NTPs were added at a concentration of 100 μM. GreA or GreB was added to a final concentration of 1 μM alongside NTP introduction. Samples were removed at various time points and quenched with an equal volume of 2× stop buffer. All remaining active PECs were chased to product by incubation with NTPs to a final concentration of 500 μM for 5 min at 37 °C.

Radiolabeled RNAs from the quenched time points were heat-denatured for 2 min at 95 °C and separated using denaturing PAGE (15% 19:1 acrylamide:bisacrylamide, 8 M urea). The gel was exposed to a PhosphorImager screen, and the screen was scanned using a Typhoon PhosphorImager. The gel images were quantified using ImageQuant software (Cytiva). For measurement of pause lifetimes, the average fraction of RNA at the pause was quantified for each time point. All measurements of the average pause RNA fraction report the average and standard deviation of time points performed in triplicate.

Pause 2 mapping and kinetics

To both map and investigate the pause escape kinetics at pause 2, a scaffold-based transcription elongation assay was designed to initiate transcription elongation upstream of the termination site D. A 10-mer RNA was used to position RNAP upstream of the sequence region where pause 2 occurs, with the 3′ G in the RNA corresponding to position 173 on the PRE sequence. The nucleic acid scaffold was annealed in a buffer (20 mM Tris, pH 7.2, and 150 mM KCl), with 5 μM RNA and10 μM T-DNA. To reconstitute the G10 ECs, RNAP was combined with the nucleic acid scaffold in transcription buffer (20 mM Tris, pH 7.2 or 8.5, 150 mM KCl, and 5 mM DTT) and incubated for 15 min at 37 °C, then the NT-DNA was added, and incubation continued for 10 min at 37 °C. The ratio of RNA:T-DNA:NT-DNA:RNAP was 1:2:5:3 corresponding to concentrations of 0.5, 1, 2.5, 1.5 μM, respectively. Next, the ECs were diluted fivefold, and heparin was added to the ECs at a final concentration of 0.1 mg/ml to sequester free RNAP. ECs were incubated with heparin for 3 min at 37 °C. To radiolabel the ECs, [α-^{32}P]ATP was added for 1 min at 37 °C, which extended the RNAs by 1 nt to form A11 ECs. To extend all ECs to A11, ECs were incubated with ATP at a final concentration of 2 μM for 3 min at 37 °C.

Reactions were initiated by adding ATP, UTP, CTP, and GTP to a final concentration of 100 μM, each. To increase pause duration, additional reactions were performed with UTP or GTP at a limiting concentration of 10 μM, with the other three NTPs at a concentration of 100 μM. $MgCl_2$ was added to a final concentration of 5 mM alongside NTP introduction. Samples were removed at various time points and quenched with an equal volume of 2× stop buffer. All remaining active PECs were chased to product by incubation with NTPs to a final concentration of 1 mM for 5 min at 37 °C.

In parallel with the transcription elongation reactions, RNA sequencing ladders were generated for precise mapping of pause locations. The ECs were prepared as described previously. The ECs were combined with ATP, UTP, CTP, and GTP to 100 μM and one 3′-deoxyNTP to 1 mM. The sequencing reactions proceeded for 20 min at 37 °C and were quenched with an equal volume of 2× stop buffer. All sequencing reactions were performed at pH 8.5.

Radiolabeled RNAs from both the quenched time points and sequencing reactions were heat-denatured for 2 min at 95 °C and separated using denaturing PAGE (15% 19:1 acrylamide:bisacrylamide, 8 M urea). The gel was exposed to a PhosphorImager screen, and the screen was scanned using a Typhoon PhosphorImager. The gel images were quantified

using ImageQuant software (Cytiva). For measurement of pause lifetimes, the average fraction of RNA at the pause was quantified for each time point. All measurements of the average pause RNA fraction report the average and standard deviation of time points performed in triplicate.

His *pause kinetics at different pH*

To investigate the pH dependence of pause escape at the *his* pause, PAGE-purified 27-mer RNA was 5′-^{32}P labeled using the same protocol implemented for the pause mapping assays (see above). The RNA positions ECs 2 nt upstream of the *his* pause site. The nucleic acid scaffold was annealed in a buffer (20 mM Tris, pH 7.2, and 150 mM KCl), with 5 μM 5′-^{32}P labeled RNA and 10 μM T-DNA. To reconstitute the G27 ECs, RNAP was combined with the nucleic acid scaffold in transcription buffer (20 mM Tris–Cl, pH 7.2 or 8.5, 150 mM KCl, 5 mM $MgCl_2$, and 5 mM DTT) and incubated for 15 min at 37 °C, then the NT-DNA was added, and incubation continued for 10 min at 37 °C. The ratio of RNA:T-DNA:NT-DNA:RNAP was 1:2:5:3, corresponding to concentrations of 0.5, 1, 2.5, and 1.5 μM, respectively. The ECs were applied to an Illustra Microspin G50 column (Cytiva) to remove unbound scaffold. Heparin was added to the ECs at a final concentration of 0.1 mg/ml to sequester free RNAP. ECs were incubated with heparin for 3 min at 37 °C. Next, the G27 ECs were diluted twofold and walked from G27 to C28 by addition of 10 μM CTP. The ECs were incubated with CTP for 1 min at 37 °C. The C28 ECs were diluted twofold and split, with half of the ECs undergoing incubation with NusA. For a subset of the C28 ECs, NusA was added to a final concentration of 4 μM (for a final concentration of 2 μM in the transcription reactions). The C28 ECs were incubated with NusA for 5 min at 37 °C. To initiate the pause escape measurements, UTP and GTP were added to the C28 ECs. UTP was added to a concentration of 100 μM, and GTP was added at a limiting concentration of 10 μM to increase pause duration. Samples were removed at various time points and quenched with an equal volume of 2× stop buffer. All remaining active PECs were chased to product by incubation with UTP and GTP to a final concentration of 500 μM for 5 min at 37 °C.

Radiolabeled RNAs from the quenched time points were heat-denatured for 2 min at 95 °C and separated using denaturing PAGE (15% 19:1 acrylamide:bisacrylamide, 8 M urea). The gel was exposed to a PhosphorImager screen, and the screen was scanned using a Typhoon PhosphorImager. The gel images were quantified using ImageQuant software (Cytiva). For measurement of pause lifetimes, the average fraction of RNA at the pause was quantified for each time point. Three replicates were performed for all time courses except for the pH 8.5—NusA condition, which only had two replicates.

Quantification of average transcription rate on the PRE

The gels were quantified with ImageJ software, and densitometry plots for both the pBR322 ladder standards and time-course samples were generated. A calibration curve was created by plotting the relative migration distance *versus* the log of transcript length for the pBR322 ladder. A linear regression was performed on this plot, generating a function to estimate transcript lengths for the time-course samples based on migration distance. For each time point, the average transcript length was determined by summing the product of each transcript length and its signal intensity and dividing the sum by total intensity. Elongation rates were determined by dividing the average transcript length by the reaction time. Rates for three independent samples were determined at both pH 7.2 and 8.5.

Quantification of pause kinetics and termination efficiency

For promoter-initiated experiments, pause kinetics were calculated as follows. The gel images were quantified using ImageQuant software (Cytiva). The band intensity for the pause RNA was divided by the total RNA, with a correction applied for major termination events prior to the pause as previously described (16). A semilogarithmic plot was generated for the average pause RNA fraction over time, and a linear regression was performed on a range of time points, starting where continued arrival of RNAP at the pause was negligible and ending before the semilogarithmic plot deviated from linearity (pause 1: 10–20 s points for pH 7.2 and 8–12 s for pH 8.5, pause 2: 14–20 s for pH 7.2 and 8–12 s for pH 8.5). Pause kinetic parameters were obtained from this regression analysis, following a published protocol for determination of pause kinetic parameters (15). All measurements of the average pause RNA fraction report the average and standard deviation of time points performed in triplicate.

To quantify the degree of termination at termination sites B and D in promoter-initiated transcription experiments, the band intensity for the termination RNA was divided by the total RNA for each individual time point. The fraction of terminated RNA was plotted over time to visualize the percentage of ECs that dissociate at termination sites B and D at both pH 7.2 and pH 8.5.

Pausing kinetics for scaffold transcription experiments were calculated as follows. The gel images were quantified using ImageQuant software (Cytiva). A semilogarithmic plot was generated for the pause RNA fraction over time (t), and a single-exponential decay fitting was performed on the plot. Pause kinetic parameters were obtained from this analysis, according to the following equation, for individual time courses (n = 3):

$$\text{Fraction of RNA at the pause} = (\text{pause efficiency}) \cdot e^{-kt}$$

Specifically, pause lifetime (or dwell time, τ) was determined as a reciprocal of the rate constant (k) for pause RNA disappearance. The reported dwell time and pause efficiency (f) for each pause is the average of individual parameters determined from fits of three individual time courses and their standard deviation.

The pause kinetics for pause 3 in the experiment outlined in Figure 4*C* were not obtained with a single-exponential decay fitting because of a poor fit. Instead, the average pause dwell time was calculated using the alternative method outlined

previously that was applied to analysis of promoter-initiated transcription experiments.

Data availability

Raw data for all experiments described in this article is available upon request to the corresponding author.

Supporting information—This article contains supporting information (References (1-11), Figs. S1–S8 and Tables S1–S4).

Acknowledgments—We thank the Landick laboratory at the University of Wisconsin-Madison for generously supplying us with expression plasmids for wild-type *E. coli* RNAP, σ^{70}, NusA, GreA, and GreB. In addition, we thank the former Mishanina laboratory members, Xing Quan, for purifying σ^{70}, and Tommy Le for assisting with the purification of GreA and GreB. We thank Dr. Ravish Sharma for purifying NusA, An Hsieh, Dr. Gairika Ghosh, and Rushabh Bhakta for assisting with wild-type *E. coli* RNAP purifications and members of our research group for their valuable feedback during the course of this study. Finally, we are grateful to Drs. Robert Landick, Daniel Roston, and Eric Strobel for critical reading of the article and helpful suggestions for improvement. All cartoons depicting the pH-responsive riboswitch RNA were prepared using BioRender. PRE secondary structure models were generated using forna (49).

Author contributions—C. S. and T. V. M. conceptualization; C. S. and T. V. M. methodology; C. S. investigation; C. S. formal analysis; C. S. writing–original draft; C. S. and T. V. M. writing–review & editing; C. S. and T. V. M. visualization; T. V. M. supervision; T. V. M. funding acquisition.

Funding and additional information—This work was supported by National Institutes of Health/National Institute of General Medical Sciences (ESI; grant no.: R35 GM142785-01), Burroughs Wellcome Fund CASI (grant no.: 1016945.01), UCSD institutional support, and Yinan Wang Memorial Chancellor's Endowed Junior Faculty Fellowship to T. V. M., and National Institutes of Health Molecular Biophysics Training Grant (grant no.: T32 GM008326) to C. S. The content is solely the responsibility of the authors and does not necessarily represent the official views of the National Institutes of Health.

Conflict of interest—The authors declare that they have no conflicts of interest with the contents of this article.

Abbreviations—The abbreviations used are: DMS, dimethyl sulfate; EC, elongation complex; ePEC, elemental paused elongation complex; nt, nucleotide; NT-DNA, nontemplate DNA; NTP, nucleotide triphosphate; PEC, paused elongation complex; PNK, polynucleotide kinase; PRE, pH-responsive element; RBS, ribosome binding sequence; RNAP, RNA polymerase; T-DNA, template DNA.

References

1. Serganov, A., and Nudler, E. (2013) A decade of riboswitches. *Cell* **152**, 17–24
2. Nechooshtan, G., Elgrably-weiss, M., Sheaffer, A., Westhof, E., and Altuvia, S. (2009) A pH-responsive riboregulator. *Genes Dev.* **23**, 2650–2662
3. Bingham, R. J., Hall, K. S., and Slonczewski, J. L. (1990) Alkaline induction of a novel gene locus, *alx*, in *Escherichia coli*. *J. Bacteriol.* **172**, 2184–2186
4. Bejerano, G., Hershberg, R., Vogel, J., Bejerano, G., Wagner, E. G., Margalit, H., *et al.* (2001) Novel small RNA-encoding genes in the intergenic regions of *Escherichia coli*. *Curr. Biol.* **11**, 941–950
5. Adeolu, M., Alnajar, S., Naushad, S., and Gupta, R. S. (2016) Genome-based phylogeny and taxonomy of the 'Enterobacteriales': proposal for enterobacterales ord. nov. Divided into the families Enterobacteriaceae, Erwiniaceae fam. nov., Pectobacteriaceae fam. nov., Yersiniaceae fam. nov., Hafniaceae fam. nov., Morgane. *Int. J. Syst. Evol. Microbiol.* **66**, 5575–5599
6. Padan, E., Bibi, E., Ito, M., and Krulwich, T. A. (2005) Alkaline pH homeostasis in bacteria: new insights. *Biochim. Biophys. Acta* **1717**, 67–88
7. Zilberstein, D., Agmon, V., Schuldiner, S., and Padan, E. (1984) *Escherichia coli* intracellular pH, membrane potential, and cell growth. *J. Bacteriol.* **158**, 246–252
8. Zeinert, R., Martinez, E., Schmitz, J., Senn, K., Usman, B., Anantharaman, V., *et al.* (2018) Structure-function analysis of manganese exporter proteins across bacteria. *J. Biol. Chem.* **293**, 5715–5730
9. Nechooshtan, G., Elgrably-Weiss, M., and Altuvia, S. (2014) Changes in transcriptional pausing modify the folding dynamics of the pH-responsive RNA element. *Nucl. Acids Res.* **42**, 622–630
10. Thomen, P., Lopez, P. J., and Heslot, F. (2005) Unravelling the mechanism of RNA polymerase forward motion by using mechanical force. *Phys. Rev. Lett.* **94**, 1–4
11. Kang, J. Y., Mishanina, T. V., Landick, R., and Darst, S. A. (2019) Mechanisms of transcriptional pausing in bacteria. *J. Mol. Biol.* **431**, 4007–4029
12. Kang, J. Y., Mishanina, T. V., Bellecourt, M. J., Mooney, R. A., Darst, S. A., and Landick, R. (2018) RNA polymerase accommodates a pause RNA hairpin by global conformational rearrangements that prolong pausing. *Mol. Cell* **69**, 802–815.e5
13. Nshogozabahizi, J. C., Aubrey, K. L., Ross, J. A., and Thakor, N. (2019) Applications and limitations of regulatory RNA elements in synthetic biology and biotechnology. *J. Appl. Microbiol.* **127**, 968–984
14. Mishanina, T. V., Palo, M. Z., Nayak, D., Mooney, R. A., and Landick, R. (2017) Trigger loop of RNA polymerase is a positional, not acid – base, catalyst for both transcription and proofreading. *Proc. Natl. Acad. Sci. U. S. A.* **114**, E5103–E5112
15. Landick, R., Wang, D., and Chan, C. L. (1996) Quantitative analysis of transcriptional pausing by *Escherichia coli* RNA polymerase: *his* leader pause site as paradigm. *Met. Enzymol.* **274**, 334–353
16. Theissen, G., Pardon, B., and Wagner, R. (1990) A quantitative assessment for transcriptional pausing of DNA-dependent RNA polymerases *in vitro*. *Anal. Biochem.* **189**, 254–261
17. Ray-soni, A., Bellecourt, M. J., and Landick, R. (2016) Mechanisms of bacterial transcription termination: all good things must end. *Annu. Rev. Biochem.* **85**, 319–347
18. Borukhov, S., Sagitov, V., and Goldfarb, A. (1993) Transcript cleavage factors from *E. coli*. *Cell* **72**, 459–466
19. Orlova, M., Newlands, J., Das, A., Goldfarb, A., and Borukhov, S. (1995) Intrinsic transcript cleavage activity of RNA polymerase. *Proc. Natl. Acad. Sci. U. S. A.* **92**, 4596–4600
20. Guo, X., Myasnikov, A. G., Chen, J., Crucifix, C., Papai, G., Takacs, M., *et al.* (2018) Structural basis for NusA stabilized transcriptional pausing. *Mol. Cell* **69**, 816–827
21. Pan, T., Artsimovitch, I., Fang, X. W., Landick, R., and Sosnick, T. R. (1999) Folding of a large ribozyme during transcription and the effect of the elongation factor NusA. *Proc. Natl. Acad. Sci. U. S. A.* **96**, 9545–9550
22. Heilman-Miller, S. L., and Woodson, S. A. (2003) Effect of transcription on folding of the Tetrahymena ribozyme. *RNA* **9**, 722–733
23. Wong, T. N., Sosnick, T. R., and Pan, T. (2007) Folding of noncoding RNAs during transcription facilitated by pausing-induced nonnative structures. *Proc. Natl. Acad. Sci. U. S. A.* **104**, 17995–18000
24. Watters, K. E., Strobel, E. J., Yu, A. M., Lis, J. T., and Lucks, J. B. (2016) Cotranscriptional folding of a riboswitch at nucleotide resolution. *Nat. Struct. Mol. Biol.* **23**, 1124–1131

25. Strobel, E. J., Cheng, L., Berman, K. E., Carlson, P. D., and Lucks, J. B. (2019) A ligand-gated strand displacement mechanism for ZTP riboswitch transcription control. *Nat. Chem. Biol.* **15**, 1067–1076
26. Steinert, H., Sochor, F., Wacker, A., Buck, J., Helmling, C., Hiller, F., *et al.* (2017) Pausing guides RNA folding to populate transiently stable RNA structures for riboswitch-based transcription regulation. *eLife* **6**, e21297
27. Cabello, C. M., Mooney, R. A., Peters, J. M., Windgassen, T., Nayak, D., Gross, C. A., *et al.* (2014) A pause sequence enriched at translation start sites drives transcription dynamics *in vivo*. *Science* **344**, 1042–1047
28. Saba, J., Chua, X. Y., Mishanina, T. V., Nayak, D., Windgassen, T. A., Mooney, R. A., *et al.* (2019) The elemental mechanism of transcriptional pausing. *eLife* **8**, 1–25
29. Abdelkareem, M., Saint-André, C., Takacs, M., Papai, G., Crucifix, C., Guo, X., *et al.* (2019) Structural basis of transcription: RNA polymerase backtracking and its reactivation. *Mol. Cell* **75**, 298–309.e4
30. Nudler, E., Mustaev, A., Lukhtanov, E., and Goldfarb, A. (1997) The RNA-DNA hybrid maintains the register of transcription by preventing backtracking of RNA polymerase. *Cell* **89**, 33–41
31. Kyzer, S., Kook, S. H., Landick, R., and Palangat, M. (2007) Direct *versus* limited-step reconstitution reveals key features of an RNA hairpin-stabilized paused transcription complex. *J. Biol. Chem.* **282**, 19020–19028
32. Tadigotla, V. R., Wagner, J., Zeh, K., Bader, M., Michel, J. B., Paul, M., *et al.* (2006) Thermodynamic and kinetic modeling of transcriptional pausing. *Proc. Natl. Acad. Sci. U. S. A.* **103**, 4439–4444
33. Zamft, B., Bintu, L., Ishibashi, T., and Bustamante, C. (2012) Nascent RNA structure modulates the transcriptional dynamics of RNA polymerases. *Proc. Natl. Acad. Sci. U. S. A.* **109**, 8948–8953
34. Landick, R. (2006) The regulatory roles and mechanism of transcriptional pausing. *Biochem. Soc. Trans.* **34**, 1062–1066
35. Strobel, E. J., Watters, K. E., Nedialkov, Y., Artsimovitch, I., and Lucks, B. (2017) Distributed biotin – streptavidin transcription roadblocks for mapping cotranscriptional RNA folding. *Nucl. Acids Res.* **45**, 1–12
36. Widom, J. R., Nedialkov, Y. A., Rai, V., Hayes, R. L., Brooks, C. L., Artsimovitch, I., *et al.* (2018) Ligand modulates cross-coupling between riboswitch folding and transcriptional pausing article ligand modulates cross-coupling between riboswitch folding and transcriptional pausing. *Mol. Cell* **72**, 541–552
37. Perdrizet, G. A., Artsimovitch, I., Furman, R., Sosnick, T. R., and Pan, T. (2012) Transcriptional pausing coordinates folding of the aptamer domain and the expression platform of a riboswitch. *Proc. Natl. Acad. Sci. U. S. A.* **109**, 3323–3328
38. Yakhnin, H., Yakhnin, A. V., Mouery, B. L., Mandell, Z. F., Karbasiafshar, C., Kashlev, M., *et al.* (2019) NusG-dependent RNA polymerase pausing and tylosin-dependent ribosome stalling are required for tylosin resistance by inducing 23s rRNA methylation in *Bacillus subtilis*. *mBio* **10**, e02665-19
39. Yakhnin, A. V., Yakhnin, H., and Babitzke, P. (2006) RNA polymerase pausing regulates translation initiation by providing additional time for TRAP-RNA interaction. *Mol. Cell* **24**, 547–557
40. Yakhnin, A. V., FitzGerald, P. C., McIntosh, C., Yakhnin, H., Kireeva, M., Turek-Herman, J., *et al.* (2020) NusG controls transcription pausing and RNA polymerase translocation throughout the *Bacillus subtilis* genome. *Proc. Natl. Acad. Sci. U. S. A.* **117**, 21628–21636
41. Saenger, W. (1984) *Principles of Nucleic Acid Structure*, Springer-Verlag, New York, NY
42. Nixon, P. L., and Giedroc, D. P. (2000) Energetics of a strongly pH dependent RNA tertiary structure a frameshifting pseudoknot. *J. Mol. Biol.* **296**, 659–671
43. Houck-Loomis, B., Durney, M. A., Salguero, C., Shankar, N., Nagle, J. M., Goff, S. P., *et al.* (2011) An equilibrium-dependent retroviral mRNA switch regulates translational recoding. *Nature* **480**, 561–564
44. Huppler, A., Nikstad, L. J., Allmann, A. M., Brow, D. A., and Butcher, S. E. (2002) Metal binding and base ionization in the u6 RNA intramolecular stem-loop structure. *Nat. Struct. Biol.* **9**, 431–435
45. Pechlaner, M., Donghi, D., Zelenay, V., and Sigel, R. K. O. (2015) Protonation-dependent base flipping at neutral pH in the catalytic triad of a self-splicing bacterial group II intron. *Angew. Chem. Int. Ed.* **54**, 9687–9690
46. Baisden, J. T., Boyer, J. A., Zhao, B., Hammond, S. M., and Zhang, Q. (2021) Visualizing a protonated RNA state that modulates microRNA-21 maturation. *Nat. Chem. Biol.* **17**, 80–88
47. Halder, A., Halder, S., Bhattacharyya, D., and Mitra, A. (2014) Feasibility of occurrence of different types of protonated base pairs in RNA: a quantum chemical study. *Phys. Chem. Chem. Phys.* **16**, 18383–18396
48. Chawla, M., Sharma, P., Halder, S., Bhattacharyya, D., and Mitra, A. (2011) Protonation of base pairs in RNA: context analysis and quantum chemical investigations of their geometries and stabilities. *J. Phys. Chem. B* **115**, 1469–1484
49. Kerpedjiev, P., Hammer, S., and Hofacker, I. L. (2015) Forna (force-directed RNA): simple and effective online RNA secondary structure diagrams. *Bioinformatics* **31**, 3377–3379